SURFACE MODIFICATION OF $LiNi_{0.5}Mn_{0.3}Co_{0.2}O_2$ CATHODE FOR IMPROVED BATTERY PERFORMANCE

A Thesis

by

THOMAS T. LYNCH

Submitted to the Office of Graduate Studies of
Texas A&M University
in partial fulfillment of the requirements for the degree of

MASTER OF SCIENCE

August 2012

Major Subject: Electrical Engineering

SURFACE MODIFICATION OF $LiNi_{0.5}Mn_{0.3}Co_{0.2}O_2$ CATHODE FOR IMPROVED BATTERY PERFORMANCE

A Thesis

by

THOMAS T. LYNCH

Submitted to the Office of Graduate Studies of
Texas A&M University
in partial fulfillment of the requirements for the degree of

MASTER OF SCIENCE

Approved by:

Chair of Committee,	Haiyan Wang
Committee Members,	Narasimha Annapareddy
	Harlan Harris
	Miladin Radovic
Head of Department,	Costas Georghiades

August 2012

Major Subject: Electrical Engineering

ABSTRACT

Surface Modification of $LiNi_{0.5}Mn_{0.3}Co_{0.2}O_2$ Cathode for Improved Battery Performance. (August 2012)

Thomas T. Lynch, B.S., University of Southern California

Chair of Advisory Committee: Dr. Haiyan Wang

This thesis details electrical and physical measurements of pulsed laser deposition-applied thin film coatings of Alumina, Ceria, and Yttria-stabilized Zirconia (YSZ) on a $LiNi_{0.5}Mn_{0.3}Co_{0.2}O_2$ (NMC) cathode in a Lithium ion battery. Typical NMC cathodes exhibit problems such as decreased rate performance and an opportunity for increased capacity exists by raising operation voltage beyond the electrolyte stability window. Very thin (~10 nm) coatings of stable oxides provide a pathway to solve both problems. As well, the electrochemical impedance spectra of the uncoated and coated cells were measured after different numbers of cycles to reveal the property variation in the cathode. Further understanding of the mechanism of rate performance enhancement and chemical protection by thin oxide coatings will continue to improve battery capability and open up new applications.

Ceria-coated Li-NMC cells show the best capacity and rate performance in battery testing. Through electrochemical impedance spectroscopy (EIS), the surface film resistance was found to remain stable or even drop slightly after repeated cycling at high

voltage. CeO_2 is proposed as a coating for Lithium ion battery cathodes owing to its high chemical stability and the demonstrated but not yet well understood electrical conductivity. Alumina-coated cathode shows comparable performance as that of the uncoated cell in the early stage of the test, but through the course of testing the rate capability and recoverable capacity is improved. This is possibly due to Al_2O_3's well-known abilities as HF scavenger and chemically inert nature. YSZ-coated cathode performs worse than the uncoated ones in terms of capacity, rate capability, and EIS-related figures of merit. The reason for the poor performance is not yet known, and repeatability tests are under way to verify performance. High voltage cycling reveals no obvious difference in irreversible loss between the coated or uncoated cells. The reason for the lack of distinction could be the relatively small percentage of surface coating compared to the thick doctor-blade processed cathode layer.

ACKNOWLEDGEMENTS

I would like to thank my advisor and committee chair, Dr. Haiyan Wang, for all of her support and guidance throughout my studies. It was extremely edifying to learn the technical and organizational ins and outs of research at the university level, and I am grateful for the opportunity she has provided me. I would also like to thank my committee members; Dr. Rusty Harris, Dr. Miladin Radovic, and Dr. Narasimha Reddy, for their participation in my research process.

I would like to especially thank my colleague Clement Jacob for all his collaboration and friendship during the short course of our research together. His intellectual honesty and relentless focus provided a sterling example. As well, colleagues Joon Hwan Lee, Fauzia Khatkhatay, and Jie Jian merit much thanks for their collaborative work in imaging. I want to also thank all the members of the Functional Thin Film Processing and Characterization group for enriching both my knowledge base and my graduate experience.

Last, I would like to acknowledge the faculty and staff of the Texas A&M Electrical and Computer Engineering department for their holistic support including a graduate teaching assistantship during my time in school.

NOMENCLATURE

TEM	Transmission Electron Microscope
SEM	Scanning Electron Microscope
EDX	Energy Dispersive X-ray
STEM	Scanning Transmission Electron Microscope
PLD	Pulsed Laser Deposition
LIB	Lithium Ion Battery
NMC	Lithium Nickel Manganese Cobalt Oxide
EIS	Electrochemical Impedance Spectroscopy
GITT	Galvanostatic Intermittent Titration Technique
CV	Cyclic Voltammetry
SEI	Solid Electrolyte Interface
YSZ	Yttria-stabilized Zirconia

TABLE OF CONTENTS

LIST OF FIGURES

FIGURE Page

FIGURE Page

FIGURE Page

LIST OF TABLES

1. INTRODUCTION

1.1 Motivation

Energy use in today's society is constantly growing, and with that growth comes a great need for advanced energy storage technologies. Diverse applications from energy storage of renewable sources including solar and wind for efficient power grid usage, to electric and hybrid electric vehicle powering, to the seemingly pervasive mobile electronics, all call for advancement in electrical energy storage systems. Typical concerns for energy storage are energy content per volume or mass, useful lifetime, rate capability, cost and safety. From grid-level energy storage to portable microelectronics, Lithium ion batteries have displayed attributes that make them advantageous. Currently, Lithium ion batteries can be seen in use in cell phones and laptop computers; most electric vehicles like the Tesla Roadster, Chevrolet Volt, and Nissan Leaf; and portable power tools. However, there is still much development needed for the relatively early stage battery technology to become advantageous over other energy storage forms. For instance, electric vehicle applications require much higher volumetric and specific capacities to truly be viable economically compared to gasoline [1]. As well, improving the rate capabilities of various Li-ion battery materials would open them up to commercial viability.

This thesis follows the style of *Journal of Power Sources.*

First, this section reviews battery history and basic operation mechanisms. Then the components of Li-ion batteries are surveyed with a focus on cathode materials and the approaches for cathode performance improvement.

1.2 Battery Background

A battery is an electrochemical system that converts chemical potential to electrical energy through reduction-oxidation (redox) reactions. These reactions which transfer charge have been exploited since early human history in such devices as the 'Baghdad battery'. Batteries have existed since the early 19th century when Allesandro Volta paired zinc and copper in a brine electrolyte. Early batteries were primary batteries (meaning single discharge use) and relied on the use of metal electrodes and acidic electrolyte such as the lead-acid battery. Knowledge in chemistry, materials science, and theoretical physics has since been developed and applied to advance the capability to electrochemically store and deliver energy. Discovery of reversible chemical reactions led to invention of secondary, also called rechargeable, batteries, from which many commercial applications have come. Fig. 1 shows the progress of battery development from the standpoints of volumetric and mass energy density. Energy density is calculated by taking a cell's operating potential in Volts multiplied by the current it produces at that potential. The total current produced by a battery is its capacity, measured in Ah/kg or Ah/l.

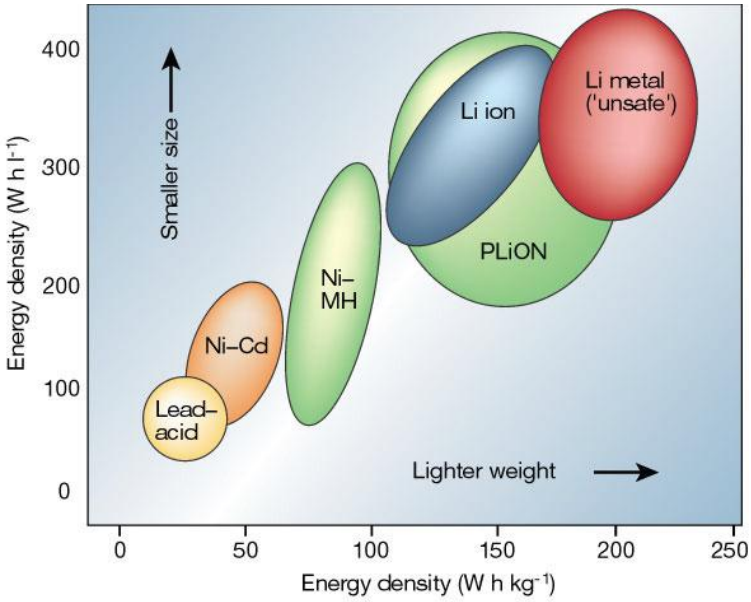

Fig. 1: Secondary battery energy densities showing high density of Li chemistry batteries compared to other conventional technologies [2].

Because of Lithium's position on the periodic table, specifically low mass (with equivalent weight 6.94 g/mol and specific gravity 0.53 g/cm^3) and high electropositivity (Li metal sits at -3.04 V versus a hydrogen electrode), it has several advantages as a material for batteries [2]. In that vein, Lithium metal batteries were created in 1976 by Whittingham [3]. These batteries used Li metal anodes with TiS_2 cathodes, and though they exploited high energy density they also experienced significant problems with safety. Li metal would build up unevenly upon cycling, eventually forming bridges across the battery which would short and possibly explode the batteries. In order to prevent the above issue, Li-ion containing materials were discovered for use as electrodes. In 1980, Goodenough *et al.* introduced $LiCoO_2$ as a layered cathode material for a so-called "rocking chair" battery [4]. Oxides are excellent candidates for Lithium

ion insertion materials because Oxygen's high electronegativity causes extremely ionic bonds which facilitate intercalation. More important oxide materials with different structures were developed later including spinel $LiMn_2O_4$ and polyanionic olivine $LiFePO_4$ [5; 6]. Commercially, Lithium ion batteries entered the market in 1991 by Sony and have found many applications and sparked much more development since then [7].

1.3 Operation Principle of Lithium Ion Battery

Batteries contain two electrodes, cathode and anode, physically separated and usually placed in on the two sides of a conductive electrolyte. Redox reactions occur at the interface between the electrolyte and the electrodes. Specifically, in Lithium-ion batteries, the reactions always involve shuttling of Li^+ ions and electrons, and the electrolyte plays no active electrochemical role except as an ionic conductor. During charging, Li^+ ions are pulled away from the cathode by an applied potential, travel through the electrolyte, and are stored in the anode. The electron associated with that ion travels in the opposite direction through the circuit to be recombined in the anode thus preserving charge neutrality. During the discharge process, the reverse happens and the Li^+ ions are naturally intercalated into the cathode due to their lower potential while the electrons travel through an external circuit producing the current. Discharge is a natural process; that is, because the lithium ions are at a lower potential when in the cathode they naturally flow from the anode to the cathode if the external circuit is closed allowing the electrons to concurrently flow. Fig. 2 is a schematic representation of the internal processes of lithium ion batteries.

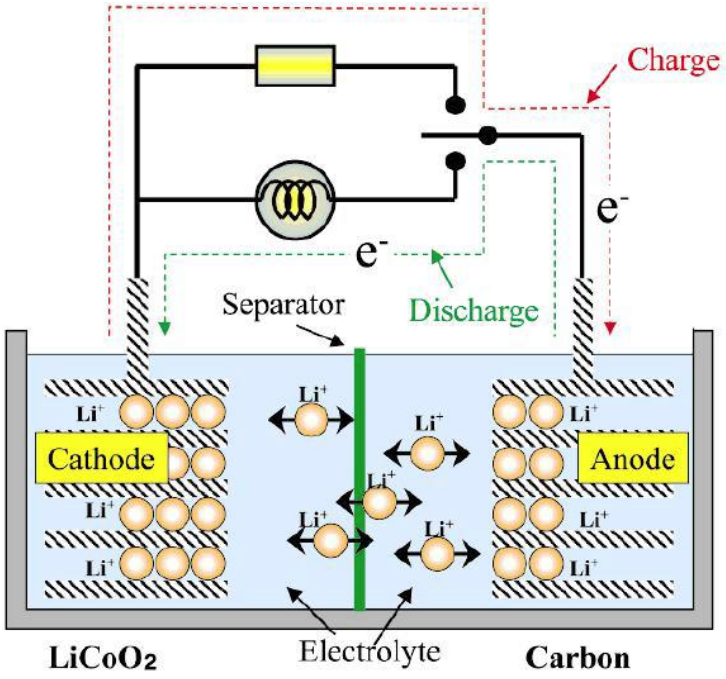

Fig. 2: Operation principle of Lithium ion battery [8]

1.4 Anode

The anode of the Li-ion battery stores the charge of Li^+ ions and electrons for discharge use. Anodes can start out containing Lithium, as in the case of Li metal. Or, they might start out without Lithium such as Carbon anodes (graphite, Carbon Black, et cetera), novel Lithium alloys or metal oxides [9; 10]. Lithium metal was the first anode used in research, but fell out of favor quickly due to its nature to form dendrites upon cycling rather than planar Lithium coatings. These dendrites could lead to shortened battery lifetime and, in some extreme cases, battery explosions. Intercalation compounds for Lithium, materials that can integrate Lithium into their atomic lattice, are now used as both anodes and cathodes in batteries.

1.4.1 State-of-the-art anode

Micrometer-sized graphite powder has been the commercial choice for anodes for most of Li-ion batteries. Graphite is carbon that forms in two-dimensional sheets bonded vertically together through van der Waals forces. This leaves planes of weak bonding where Lithium can easily penetrate and be stored. Graphite has a capacity around 370 mAh/g which is higher than most cathode materials [7]. Because Lithium inserts into graphite at around 1 V relative to Li+/Li which is unstable to the electrolyte, solid-electrolyte interfaces (SEI) always form a passivation layer which consumes anode volume and reduces capacity [11]. There is a tradeoff underlying graphite surface area selection which on one hand increases power capability by allowing higher rate reactions but on the other hand consumes more capacity from SEI formation. Decreasing graphite particle size through novel shapes such as microbeads or carbon fiber continues to receive research interest, although it is doubtful that any enhancements will be significant enough to break the inertia of commercial anode production. Coating a graphite anode with conductive metals such as Ag, Zn, or Sn has been shown to increase intercalation/deintercalation reaction rate [12]. This is due to a different anode/electrolyte interface than normal graphite's organic SEI. The metal interface proves electrokinetically favorable and aides high rate charging and discharging.

1.4.2 Next generation anodes

A more inventive high capacity anode can be found in Lithium metal alloys. In early batteries Aluminum was used as a replacement anode for Li metal as it was found that the two metals could alloy while still providing similar voltage reactions and

preventing the dendrite problem [2]. However, these anodes did not last long as they experienced large volume changes during cycling and pulverized themselves. In fact, anodes that display high capacity by storing more than one Lithium ion per stoichiometric unit of anode suffer from this high volumetric change due to simple physics. Eventually as a result of the volumetric changes the anode loses electrical contact with current collector. Pure Aluminum- and Tin-Lithium alloys were abandoned in favor of composites which could hold stable regions of inactive metal and active alloy metal regions. Metal composites such as Cu_2Sb or InSb and other composites like Sn-Fe-C were studied to this end, but either sacrificed capacity through Li_2O formation or did not show enough long-term cyclability [13].

1.4.3 Nanomaterials for anodes

The advent of nanotechnology has made viable several interesting materials as anodes in Lithium ion batteries. For instance, amorphous Tin Oxide was found to readily accept Li+ ions and had about twice the capacity of graphite, but suffers from pulverization upon cycling due to large volume changes [14]. One solution to the pulverization was to try to limit the intercalation to two dimensions. SnO_2 single layer sheets were then fabricated to alleviate the high volume change [15]. Silicon saw the same opportunity (>10 times graphite's capacity) and pitfall (400% volume change upon cycling), which was overcome through Si nanowires as an anode to accommodate the strain [16]. Fig. 3 shows nanowires' tolerance of volumetric change without pulverization compared to conventional thin film or powder morphologies.

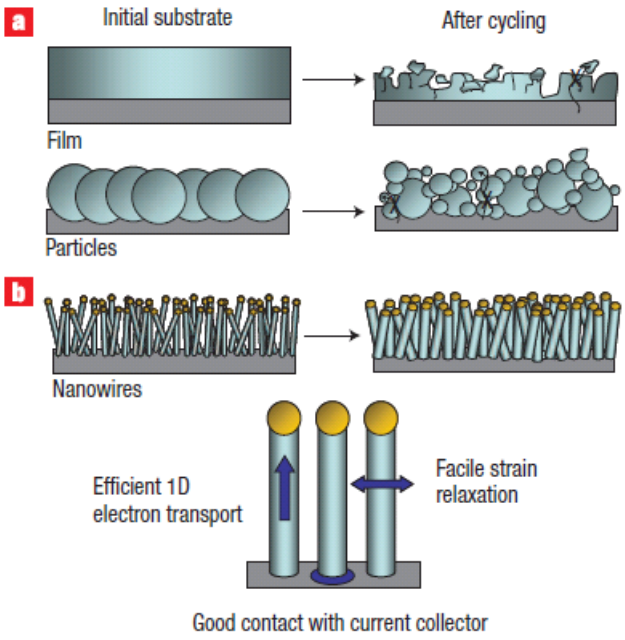

Fig. 3: Different morphologies for anode and results after cycling [16].

1.5 Electrolyte

1.5.1 Conventional liquid electrolytes

The electrolyte is the component in Lithium ion batteries that allows ion transport between the two electrodes. Its critical features are ionic conductivity, chemical and electrochemical stability, and safety [7]. Electrolytes in commercial batteries are typically composed of salts dissolved in liquid organic solvents. The most conventional electrolyte involves the salt $LiPF_6$ and a solvent of ethylene carbonate (EC) with either dimethyl carbonate (DMC) or diethyl carbonate (DEC) and allows ionic conductivity of above 10 S/cm. Solvent choice affects ionic conductivity through solvent dielectric constant which indicates how well a salt will be solvated and viscosity which influences

mobility [17]. In addition, the solvent's melting point should be low enough that operation conditions do not threaten phase change and the boiling point should be high enough that safety can still be assured. EC in solution is what forms the SEI at the anode during first charge at around 0.8V with respect to Li^+/Li [18]. Some of the main constituents of the SEI include Li_2CO_3 and Li_2O. This passivating film is critical to prevent solvent from penetrating and dissolving the anode. A different passivating film is formed at the cathode at higher voltage through oxidative processes in the electrolyte. Several different additives are used in the electrolyte solution for different purposes including improving SEI formation, improving wettability to separator, and enhancing thermal stability [19].

1.5.2 Solid electrolytes

Solid electrolytes confer many advantages over liquid such as natural cell sealing, pressure/temperature variation resistance, better electrochemical stability, and better safety [17].There are two types of solid electrolytes; solid inorganic electrolytes and solid polymer electrolytes. Solid inorganic electrolytes consist of crystalline or glass frameworks, and display poor ionic conductivity (see Table 1). All solid-state batteries are restricted to thin film due in part to the poor conductivity of the electrolyte. The traditional view on solid polymer electrolytes was that they could only be conducting in an amorphous state above their glass transition temperature; however, crystal complexes made of salts dissolved in polymers have been shown to be ionically conducting [11]. The challenge in the field now is achieving comparable ionic conductivities to liquid electrolytes, moving from 10^{-7} up to 1 S/cm.

Table 1: Various electrolyte system ionic conductivities[17]

Medium	Chemistry	Ionic Conductivity (S cm-1)
Liquid	$LiPF_6$:EC/DMC	10.7
	$LiClO_4$:EC/DMC	8.4
Solid Polymer		8.0×10^{-8}
Solid State	crystalline LISICON	5×10^{-4}
	glass LIPON	8×10^{-7}

1.6 Cathode

Cathodes in Lithium ion batteries have seen much development as well due to materials research. Unlike Carbon anodes, which have dominated the commercial market, several different cathodes have been favored over the short history of Lithium ion batteries. In general, battery systems require from cathodes that they:

1. Be composed of readily reducible/oxidizable ions, e.g. transition metals;
2. React with lithium reversibly;
3. Have a high energy of reaction with Li (capacity and voltage);
4. React with lithium rapidly both on intercalation and deintercalation;
5. Be a good electronic conductor;
6. Remain stable when contacted by an electrolyte;
7. Possess a low cost and be easily synthesized; and
8. Be environmentally benign [20].

1.6.1 Layered intercalation cathodes

The first materials used in LIB's in the mid-1970's were dichalcogenides such as TiS_2 [7]. TiS_2 cathodes displayed reversible intercalation above 2 V and had problems with deposition on Li anodes they were paired with, which necessitated new materials. In 1980, the structurally stable cathode material $LiCoO_2$ with reaction voltage around 3.8 V was proposed [4]. It has become the most commercially accepted cathode due to its high energy capacity and relative stability. Many different transition metal oxides including Nickel and Manganese are able to form this layered rock salt structure (seen in Fig. 4). Lithium forms planes that layer with planes of edge-sharing CoO_6 (or NiO_6, or MnO_6) octahedra, allowing Li to diffuse in two dimensions. Diffusivity can be found in Table 2 along with that of the other common cathode structures. Due to the metals' different binding energy with oxygen they display different cycling characteristics such as reaction potential and stable lithiation range, of which Co has proven most advantageous. $LiCoO_2$ is stable until delithiated past the composition $Li_{0.5}CoO_2$, at which point it undergoes a Jahn-Teller distortion into a different phase which prevents intercalation, resulting in lost capacity [21]. This phase change from monoclinic to hexagonal is accompanied by a volume change around 9% that can deteriorate electrical contact among grains [22]. Therefore, $LiCoO_2$ batteries are only cycled between Li and $Li_{0.5}$ in composition (about 3 V to 4.2 V) which leaves around 140 mAh/g of capacity. Another problem with this material is that when trying to charge to high voltage (above 4.2V), Co^{4+}/Co^{3+} ions can dissolve in the battery's electrolyte.

1.6.1.1 $LiNi_{1-x-y}Mn_xCo_yO_2$ type cathodes

Lithium Cobalt, Nickel, and Manganese Oxides all exist in the layered structure, and all three of these transition metal oxides are able to form a solid solution with one another. Alone, $LiNiO_2$ batteries saw high capacity but poor lifetime due to cationic mixing of the metal and Li layers. Layered $LiMnO_2$ quickly devolves into spinel material when charged to a useful capacity, but is cheap. Finally, $LiCoO_2$ performs stably but has issues of cost and toxicity. Many studies have been done in combining Ni and Co [23; 24], Ni and Mn [25; 26], and all three [27; 28]. Nickel and Manganese cost less and are less toxic than Cobalt, but layered materials with just these two elements have problems of very low electronic conductivity. The addition of Cobalt increases structural stability due to its higher strength ionic bonding, which manifests in larger capacity, higher rate capability, and longer cell lifetime. The process of balancing materials that substitute out Cobalt while still maintaining capacity and rate capability has created layered cathodes which are potential next generation cathode materials. $Li(Ni_{0.33}Mn_{0.33}Co_{0.33})O_2$ is a heavily studied layered cathode material that utilizes the aforementioned benefits.

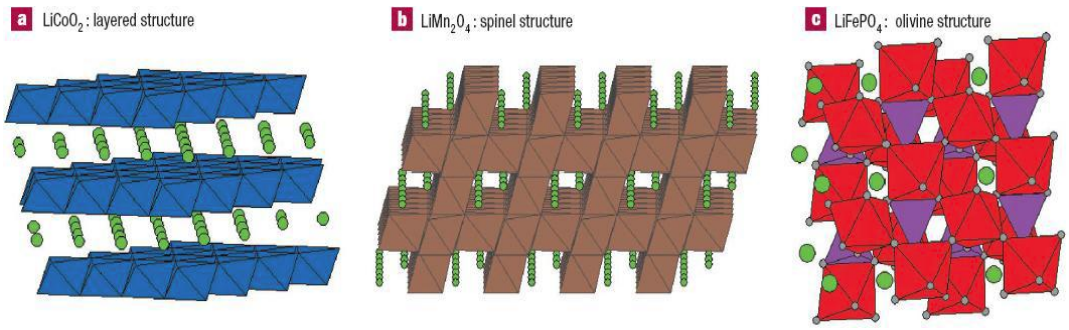

Fig. 4: Li-containing oxide cathode materials crystal structures with Li as green dots [29].

1.6.1.2 Spinel structure cathode

Spinel $LiMn_2O_4$ was proposed in 1983 by Thackeray as a cathode material [5]. The spinel structure involves cubic close-packing of the metal-oxide octahedral but the Li ions are arranged in a 3-D column instead of 2-D planes. This structure prevents large species from inserting into and blocking Li conducting channels and also changes volume less upon cycling [21]. Lithium Manganese Oxide has the advantages of low cost, non-toxicity, both good electronic and lithium ion conductivity and a structure (seen in Fig. 4) that gives great three-dimensional stability. The main disadvantage of this material is its large capacity fade due to several mechanisms such as incomplete Jahn-Teller distortion or phase change upon delithiation causing mismatched grains [30] and Mn dissolution and Oxygen loss into the electrolyte especially at the high voltage plateau around 4 V [31]. Unfortunately, these effects are exacerbated by decreasing the cathode particle size (and thus surface area to volume ratio). Methods have been devised to prevent capacity loss; namely stoichiometry modification, structural doping mainly with Al, and nanoscale coatings which will be detailed in Section 1.7 [32; 33].

1.6.1.3 Olivine structure cathode

The olivine structure containing 3-D columns of Li conduction was also proposed as an improvement over layered $LiCoO_2$. The olivine phase was theorized in 1989 and $LiFePO_4$ was introduced in 1997 by Padhi et al and enjoys benefits such as high energy capacity (170 mAh/g theoretical capacity and 3.5 V reaction), low cost, good cyclability, and safety [6; 34].The structure is more stable than others because Oxygen ions form strongly bonded PO_4 tetrahedra which causes valence state of the metal to have less impact on lattice parameters [35]. Its main disadvantage is its very poor electronic conductivity several orders of magnitude lower than other conventional cathode materials [36]. The low conductivity means that capacity is diminished even at moderate rates, and for high rate applications such as electric vehicles capacity would be severely limited. Small particle size is critical for increasing electric performance of $LiFePO_4$ cathodes and other methods are employed to improve its kinetics. Table 2 displays a comparison of figures of merit of the main first generation cathode material structures.

Table 2: Comparison of conventional cathode material properties [17; 37].

	$LiCoO_2$	$LiMn_2O_4$	$LiFePO_4$
Avg. voltage (V)	3.84	3.86	3.22
Energy density (Wh kg^{-1})	193.3	154.3	162.9
Energy density (Wh L^{-1})	557.8	418.6	415
Practical capacity (mAh g^{-1})	140	120	170
D_{Li} (cm^2/s)	10^{-10} to 10^{-8}	10^{-11} to 10^{-9}	10^{-14} to 10^{-15}
σ (S/cm)	10^{-4}	10^{-6}	10^{-9}

1.7 Cathode Performance Improvement Methods

Several strategies exist to increase certain aspects of performance of all cathode materials. The most prevalent method to increase rate capability involves decreasing grain particle size. By decreasing the diffusion length required for Lithium ions, they can be more quickly inserted and extracted en masse. Typically grain size has been on the order of tens of micrometers, but for high rate applications especially in poor conducting $LiFePO_4$ grains have been created on the order of nanometers. The drawback to smaller particle size is that increased surface area increases reactivity between the electrolyte and the cathode. This means that solid-electrolyte interface formation is increased along with its pronounced capacity fade, and also particle to particle electronic contact becomes problematic [11].

Substitution doping is another method used to improve battery performance. When doped in Li sites such as in layered materials, Mg or Zr can increase the structural stability and allow more percent Lithium to be extracted, increasing the capacity and lifetime [38]. However, doping in Lithium sites by its very nature decreases potential capacity. Instead, structural doping of the metal cation such as in $LiCoO_2$ creates similar benefits by playing with lattice parameters. In fact, this is how the next generation material $Li(Ni_{0.33}Mn_{0.33}Co_{0.33})O_2$ was discovered. For the spinel material $LiMn_2O_4$, doping the Mn position with rare-earth elements has been found to decrease lattice parameter and in turn improve structural stability and enhance rate capability and cyclability [39]. In the case of $LiFePO_4$, many different metals doped in the Fe position have been found to increase the rate capability, though the mode is still controversial [40]. The last method available to enhance rate capability is through coating the cathode with a thin layer of metal, oxide, Carbon, polymer, or other material.

1.7.1 Cathode coatings

1.7.1.1 Coating overview

Nano-scale surface coatings are an important technique to improve the performance of cathodes in Lithium ion batteries. Because much of the important reactions in battery operation happen at interfaces, surface coatings offer efficient solutions to several different problems of different cathode materials such as preventing damaging phase changes or allowing higher voltage cycling by protecting against chemical reactions. Cathode particle size reduction is a standard method to enhance performance by reducing diffusion length of Li ions. However, most advanced materials

already utilize nano-sized particles and no more improvement can be gained on that front. Substitutional doping is another improvement method which stabilizes cathode structure by replacing either Li or other cation sites with a small percentage of other cations. This can enhance rate performance by changing Li-conductive channel size due to changing interatomic potentials. With larger conductive channels, the material is able to shuttle Li ions in and out faster. Doping can also enhance cyclability through increased structural stability of non-deintercalating cations in Li sites. This would result in batteries able to cycle longer before mechanical failure and also batteries able to cycle at higher potentials due to being able to use a larger percentage of Li ions. The cost of substitutional doping in Li sites is a decreased capacity. Surface coatings are on such a small scale that they do not appreciably reduce volumetric or gravimetric capacity, and thus are an important method of improvement for lithium ion batteries.

1.7.1.2 Fabrication methods

Several different fabrication methods have been used to coat nanometer scale layers on cathodes. A solution deposition step involving precursor sonication in solvent followed by annealing to decompose is very common for many coating chemistries [41-43]. However, it can result in a mixed layer of cathode and coating on the surface, depending on anneal temperature and time, causing initial capacity loss. Sol-gel methods carry the same danger of diffusing into the active material. In addition, chemical coating methods provide only loose control over coating thickness. Average thickness is determined after the fact of reaction by imaging techniques, and different coatings are characterized by weight or molar percent of solution before reaction. Besides the simple

mechanical and chemical methods, there are more precise deposition techniques. Atomic layer deposition (ALD) has been applied to precisely control growth to the level of monolayer [44]. This method allows controllable thickness down to sub-nanometer range. Another method allowing control over coating thickness is pulsed laser deposition (PLD), whereby a target is ablated by a pulsed laser [45]. Deposition conditions and substrate selection determine film stoichiometry, crystallinity, and thickness. Another physical deposition method used to deposit on cathodes is magnetron sputtering [46]. PLD, sputtering and ALD do not require an anneal step to ensure correct coating chemistry.

1.7.2 Coatings on $LiCoO_2$

The most commercially prevalent Li ion battery cathode is $LiCoO_2$. Even with its high structural stability compared to other cathode materials, there is capacity loss associated with cycling the cathode. This loss is attributable to different factors. Both structural reordering through Co – Li lattice site switching and a phase change from hexagonal to monoclinic ordering around 4.2V affect the cathode's capacity [47]. Due to internal strain, microcracks form during cycling that ultimately physically erode the battery and result in loss. Doping lattice sites with Al or Mg is sometimes reported to provide more structural stability, but at the cost of capacity from substitution of Lithium [48-50]. However, surface coatings have proven to significantly delay cycling capacity loss, leading to a longer battery life. This mechanism can be seen in so-called 'zero strain' coatings. They are thought to prevent the anisotropic volume changes through surface stress on the active material. In theory, if the coating material is extremely

strong, then it will prevent the cathode from exhibiting strain. Many transition metal oxides have been tested and found to be especially good for this purpose, including MgO, Al_2O_3, and ZrO_2 [45; 51; 52].

MgO has been demonstrated to work well in a surface coating even as an amorphous film [53]. This means that extremely ordered interface stress preventing cathode strain is unlikely. Rather, surface Mg^{2+} ions have radii very close in size to the Li^+ ion radius, which allows them to enter the layered cathode structure and fill Li^+ ion vacancies, stabilizing it even in delithiated states. With this effect, MgO coated $LiCoO_2$ batteries are able to charge to greater potential and achieve higher capacity with longer life than uncoated samples. Cyclic voltammetry curves have proven that a hexagonal to monoclinic phase transition still takes place at the same potential, yet somehow the coating prevents fracture and capacity loss [45].

Tension between Al_2O_3 and the $LiCoO_2$ cathode at its surface has also been theorized to restrict the hexagonal to monoclinic phase transformation while cycling. For this reason many different methods of ultrathin Al_2O_3 coatings have been applied. A popular method for precise thickness control is atomic layer deposition, which has been applied at different thicknesses to show that extremely thin layers (2 molecular layers) work the best for cyclability [44]. Thin films have also been created by RF sputtering, paired with LiCoO2 deposited on a Pt current collector [54]. Fig. 5 shows the magnitude of capacity retention improvement in an Al_2O_3-coated thin film cell. Al_2O_3 coating by sol-gel method at a low anneal temperature of 400 C has been shown to prevent a

hexagonal-monoclinic phase transition [55]. Coatings that were too thick resulted in lost capacity by acting as a large insulating layer between the active material and electrolyte.

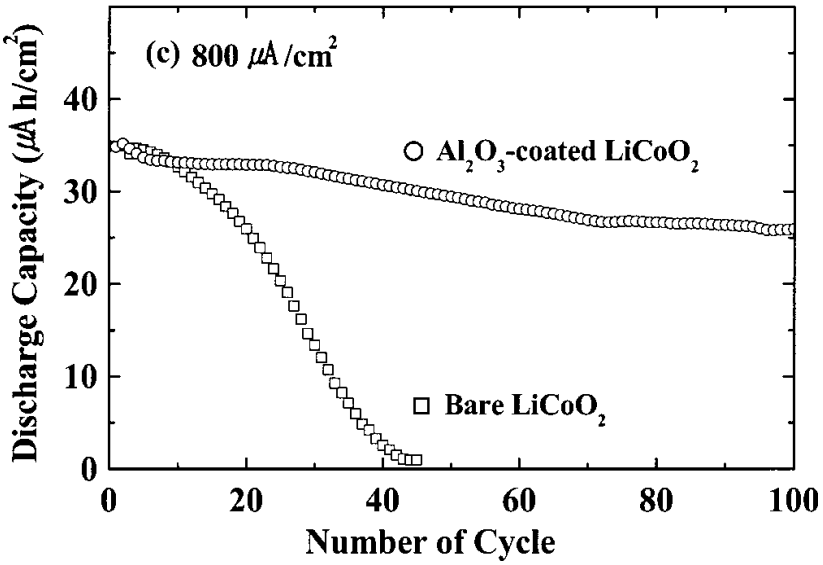

Fig. 5: Capacity retention improvement of Al_2O_3 coating on thin film $LiCoO_2$[54]

ZrO_2 was chosen as a surface coating material due to its large fracture toughness, in the hopes that it would be able to handle or prevent the large anisotropic volume changes that accompany cycling [52]. Results of ZrO_2 coatings showed the same qualitative lifetime enhancement, but further X-ray diffraction testing showed that volume changes on cycling proceeded the same with or without ZrO_2 coating [56]. Thus, the so-called 'zero strain' mechanism does not exist as an inhibitor of normal cycling strain.

Another opportunity that surface coatings can create for $LiCoO_2$ cathodes is the unlocking of higher potentials for cycling, and thus higher capacity and energy densities. Without coatings, at high potentials (typically above 4.2 V) the cathode undergoes

several chemical reactions with the electrolyte at the solid-electrolyte interface (SEI). A surface coating of a material chemically inert to the electrolyte is able to shield active material from reactions. The main mechanism seen in electrolyte reactions is dissolution of Co^{4+} ions from the active material [53]. Evidence has shown that coatings prevent a higher oxidation state from forming on incorporated oxygen, which is a chemical basis for decomposition [57]. When sized on the nanoscale, coatings do not significantly impede cell kinetics. Important materials chosen for coating $LiCoO_2$ to prevent electrolytic dissolution include Al_2O_3, ZrO_2, CeO_2, TiO_2, MgO and YSZ [41; 50-52; 58-60]. Al_2O_3 has been shown to form a passivating layer of AlF_3 in contact with $LiPF_6$ salt in electrolyte [61]. This product neutralizes HF in electrolyte thus preventing loss of capacity by etching. YSZ also creates a different SEI which has been show to impede cathode dissolution [59].

1.7.3 Coatings on $LiMn_2O_4$

$LiMn_2O_4$ spinel cathode materials are considered another potential option for main stream Li-ion batteries because they are cheap, environmentally safe and have high energy capacity. Much promise is seen particularly in the affordability, as they are 5-6 times cheaper than conventional $LiCoO_2$-based batteries while still maintaining moderate capacity (~135 mAh/g) [62; 63]. However, these cathodes encounter problems of capacity fading due to several different mechanisms especially at higher temperature. Namely, cycling through the 3 V peak causing Jahn-Teller distortion and an associated phase change and also problems with electrolyte reacting with/dissolving both Mn^{4+} and O^{2-} ions destroying the structure cause capacity loss throughout cycling [64; 65]. Both of

these problems can be effectively mitigated through surface coatings of the active cathode material.

In order to provide structural stability and chemical protection, several different metal oxides have been coated on $LiMn_2O_4$ through sol-gel or coprecipitation methods. Al_2O_3 coating formed through an acidic sol-gel showed little difference from bare performance, and an improperly prepared sample saw rapid capacity loss from processing acids [66]. However, this experiment probably saw poor results due to ineffective coating of cathode, and lacked long-term or high temperature results where fading is more visible. ZrO_2 was also used as a coating and exhibited enhanced rate performance due to reduction of reaction impedance and also inhibition of lattice structure fluctuations upon cycling [67]. Fig. 6 shows results of a rate capability test displaying ZrO_2's improvements of stability.

Amorphous ZrO_2 was also applied by pulsed laser deposition onto thin films of $LiMn_2O_4$, and enhanced the kinetics of battery reactions long-term by preventing dissolution [68]. MgO coatings have been shown in one comparative study to be more effective at room temperature capacity retention than several other Li containing metal oxides as well as Al_2O_3; however, in another study Al_2O_3 was reported with better specific capacity and retention [64; 69]. Obviously coating thickness optimization plays a role in effectiveness, so care should be taken in preemptive conclusions of relative efficacy. All coatings on $LiMn_2O_4$ have been shown to reduce charge transfer resistance and delay or prevent capacity loss due to Mn^{3+} dissolution or structure distortion.

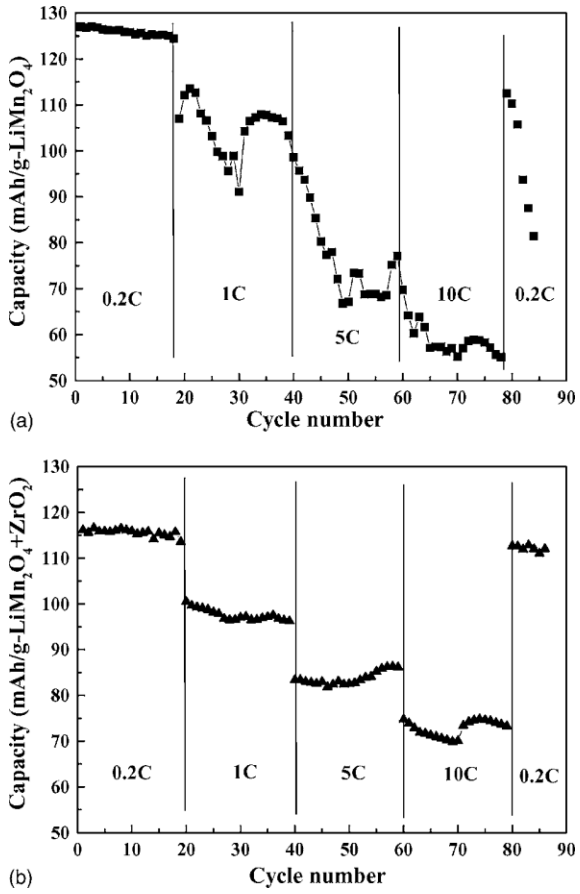

Fig. 6: Rate capabilities of bare and ZrO_2 modified cathodes [67].

1.7.4 Coatings on $LiFePO_4$

Lithium iron phosphate ($LiFePO_4$) is seen as a potential next generation battery cathode for its high theoretical capacity (140 mAh/g), thermal stability, low cost of iron compared to cobalt, good capacity retention, and environmental safety [6]. However, it has poor electronic conductivity and Li diffusion constant, and the poor charge transfer kinetics lead to unobtainable capacity that is exacerbated at higher cycling rates. One concern is optimizing particle size of $LiFePO_4$ for enhanced diffusivity/conduction, but

also several different surface coatings can be applied to improve performance. The most widely used conductive coating for $LiFePO_4$ is Carbon. Through many different methods, on many different types of cathode (particle and thin film), Carbon has been shown to greatly enhance electronic conductivity and thus increase rate capability [70-73]. Fig. 7 shows the difference of cycling curves between coated and uncoated. The increased flatness of the charge and discharge curve indicates a steady, more uniform change of phase between $LiFePO_4$ and $FePO_4$ than the uncoated.

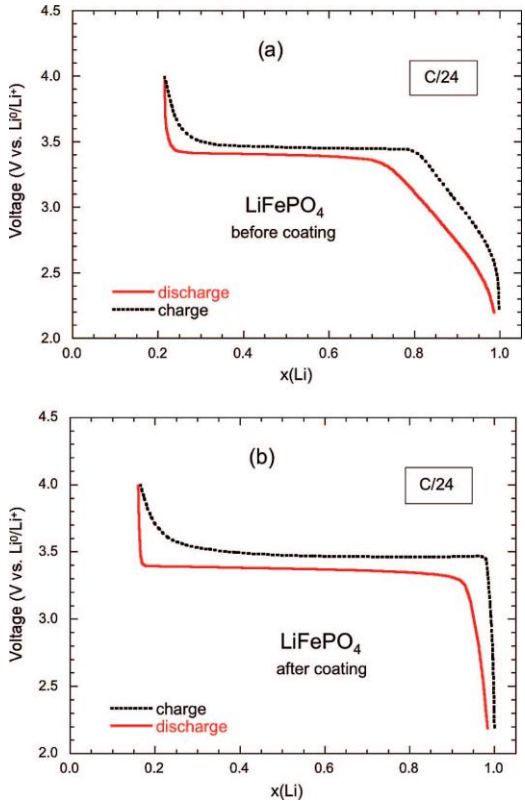

Fig. 7: $LiFePO_4$ cycling curves with and without carbon coating [71].

In addition to evidence such as flatness of voltage plateau or increased capacity at higher rates from the cycling curves, Carbon coated cathodes show cyclic voltammetry curves with extremely localized current peaks at the reaction voltages around 3.4 V. Coupled with electrochemical impedance spectroscopy data showing smaller charge transfer resistance, Carbon coatings have clearly been proven to enhance the kinetics of battery performance.

Other coatings, especially oxides, have also been tested on $LiFePO_4$. SiO_2 was applied to powder by a sol-gel method to enhance ionic conductivity and reduce capacity fading by increasing thermal stability [74]. Cycled at 0.1C, SiO_2 coated cathodes achieved nearly 160 mAh/g, and at 1C capacity dropped only to about 145. This is slightly improved compared to the optimized Carbon methods, and it is speculated that the increased capacity comes from better structural stability due to the SiO_2 surface layer. TiO_2 was also used as a sol-gel coating for the same reasons [75]. This coating however did not improve capacity; rather, in a battery with Carbon anode it saw no improvement compared to an uncoated sample. In fact, it was shown that this coating had no effect on the fundamental reaction of lithiation/delithiation but the coating was able to better prevent high temperature (55° C) capacity loss in a half-cell with Li anode. Finally, CeO_2 was chosen due to its known ability to form interfaces with high electronic conductivity with other oxides. CeO_2-coated $LiFePO_4$ through a solution coprecipitation method enhanced capacity and decreased impedance while not altering the crystalline structure [76]. As well, the improved electrical contact between CeO_2-coated $LiFePO_4$ particles was shown to reduce polarization and facilitate the lithiation/delithiation

reaction [77]. Oxide coatings have been shown to improve performance of $LiFePO_4$ in some cases even better than carbon, but in general would probably be less useful for mass-production due to cost unless for a specific purpose such as a high-temperature application.

1.7.5 Coatings on $Li(Ni_xMn_yCo_{1-x-y})O_2$

$Li(Ni_xMn_yCo_{1-x-y})O_2$ cathode layered materials are seen as a viable replacement for $LiCoO_2$ in that Ni and Mn substitution enhances capacity and thermal stability while lowering cost and maintaining rate capability. Assuming appropriate particle size for favorable kinetics, a thin surface coating can make Li-NMC perform even better in several areas. For high-rate batteries, coatings of conductive material can enhance available capacity. As well, chemically stable metal oxide coatings can protect the active cathode material from dissolution by electrolyte. At higher potentials, these coatings can prevent HF etching and thus allow more reversible capacity.

1.7.5.1 Carbon coatings

Carbon coatings have been used on several Ni/Mn/Co combination layered structure cathodes in order to enhance available capacity and rate capability. $LiNi_{0.5}Mn_{0.5}O_2$ has been fabricated through coprecipitation and coated with sucrose and starch which leaves a carbon coating after annealing [78]. This carbon coating affects the cathode mainly by enhancing surface conductivity and through surface modification, whereby carbon bonds with the cathode surface rather than impurities. Increased conductivity results in shifting of charge peaks to lower voltage and discharge peaks to higher voltage indicating less domain polarization [46]. This carbon has been theorized

to also retard HF etch on the solid-electrolyte interface, which would allow higher capacity retention by preventing dissolution. Li-NMC has also benefitted from a carbon surface coating though the method of improvement is not agreed upon [79; 80]. Both experiments used liquid mixing of NMC and a sugar then annealed that mixture to obtain the carbon coating with thickness determined by weight percent. Most likely, Carbon's surface conductivity affects the enhanced rate capability of coated cathodes and surface chemistry plays a role in the enhanced reversible capacity retention. More recently, Carbon has been coated onto NMC through magnetron sputtering [46]. The purpose of the sputtering was to gain precise control over coating thickness and surface conditions. It was shown through EIS that carbon coating effectively inhibited SEI layer formation with electrolyte.

1.7.5.2 Al_2O_3 coatings

Aluminum based molecules have played a large role in coating NMC cathodes for enhanced cycle lifetime. The initial study found that a 5nm Al_2O_3 coating acts as a sacrificial protective layer to prevent HF contact with the NMC [81]. Fig. 8 shows transmission electron microscope (TEM) images of the preserved Alumina coated layer after cycling. These results are comparable to Al_2O_3 coatings on other layered cathodes, and allow battery cycling at higher potentials than the electrolyte's stability window. Not only does the Alumina layer prevent direct contact between HF and NMC (thus etching and capacity loss), but also Al_2O_3 reacts much less with the etchant requiring thinner coatings than a sacrificial Li-layered oxide would to accomplish the same purpose.

Images were taken after cycling of bare and Al_2O_3 coated cathode particles and a clear difference can be seen in terms of particle cohesion.

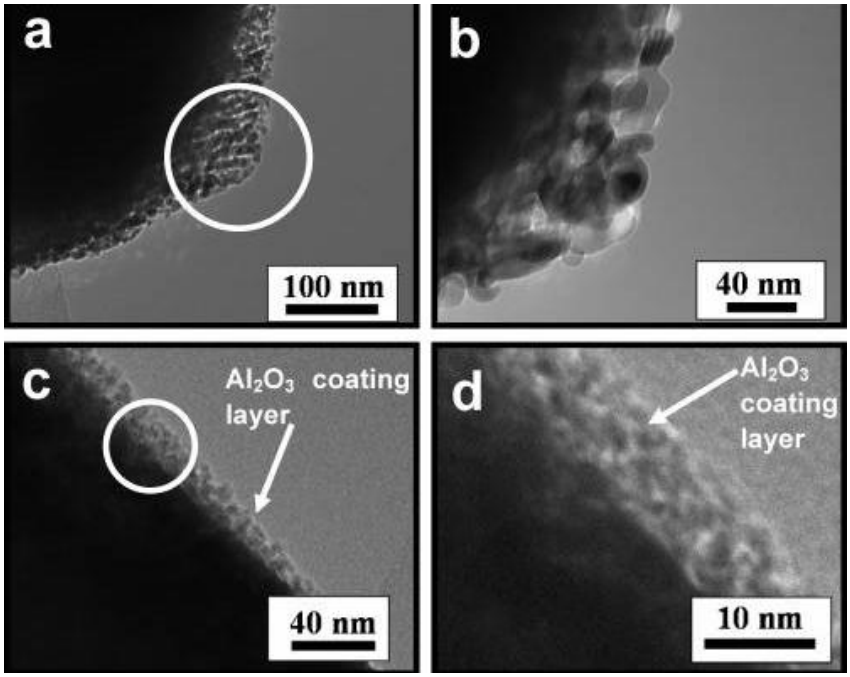

Fig. 8: TEM images after cycling of bare (a, b) and Al_2O_3 coated (c, d) cathode particles [81].

The resulting lack of cohesion separates cathode active material from conducting additive (Carbon powders) which decreases available Li ions especially in high-rate applications. Another study of solution deposited Al_2O_3 coating on NMC attributed better long term cycling with a small amount of specific capacity compared to other coatings (ZrO_2, TiO_2) [82]. Coatings of Alumina have been applied to NMC mainly by two different methods: sol-gel, atomic layer deposition [83]. ALD coatings have achieved much improved results due to the ability to fine-tune coating thickness and thus charge transfer kinetics while still retaining the HF scavenging benefit. This can be seen

in EIS results whereby charge transfer resistance of ALD Alumina coated samples as thin as four atomic layers does not change, indicating that the surface of the cathode is unaffected by electrolyte byproduct etching. Fig. 9 shows tabulations of figures of merit calculated from EIS results, and highlights the charge transfer resistance enhancement from coating. The battery's improved kinetics result in the electrochemical performance enhancement.

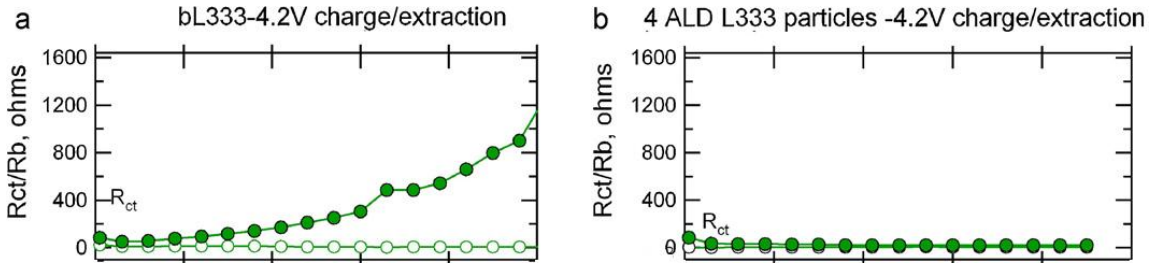

Fig. 9: Charge transfer resistance vs. cycling for uncoated (a) and Alumina coated (b) cells [84].

Other Al-containing molecules have been used as cathode coatings for HF protection including AlF_3 and $Al(OH)_3$, and $LiAlO_2$. AlF_3 is the product of HF etching Al_2O_3, and thus is more stable to HF than Al_2O_3. Coatings of AlF_3 synthesized by coprecipitation showed comparable results to Al_2O_3 in terms of long-term capacity retention and improved first-cycle capacity retention [85]. $Al(OH)_3$ has also been coated through solution methods to protect the cathode at higher temperature and enhanced rate capability [86; 87]. Lower charge transfer resistance R_{ct} was seen in coated samples that had improved capacity retention at higher rates. As well, improved thermal stability resulted. $LiAlO_2$ was used as a coating because its Li content would allow high Li

diffusivity and the Al content could serve as an HF scavenger [83]. It performed better in long-term, high rate capacity retention than an Al_2O_3 coating due to the several different effects it allows.

1.7.5.3 ZrO_2 coatings

Zirconium Oxide is a widely used coating for other layered transition metal oxide cathodes, and NMC is no different. Cycling at high voltage can be less destructive with the very stable Zirconia to prevent Cobalt dissolution and other electrolyte side reactions. A comparative study found that a solution-based ZrO_2 coating had the best capacity retention at low rates and lower charge transfer resistance after 100 cycles compared to Al_2O_3 and TiO_2 coatings [82]. Other studies report increased thermal stability, better rate capability, increased capacity retention, and decreased charge transfer resistance compared to pure NMC cathodes [88; 89]. Though one of these trials induced an inert Li_2ZrO_3 coating, both were able to realize an optimized protective layer due to the strong Zr-O bond. Another hypothesis is that some Zr from the coating penetrates into the cathode in Li sites and helps stabilize the structure, also increasing lattice parameters which would help battery kinetics [88].

1.7.5.4 TiO_2 coatings

Titanium Oxide is another stable metal oxide compound that can coat and protect cathodes. In different studies, an optimized TiO_2 coating on NMC has been shown to increase initial capacity and allow more capacity at higher rate (through enhanced transport mechanism), and also to decrease impedance after long amounts of cycling (by preventing side reactions with the electrolyte) [90; 91]. In a comparative study,

however, TiO_2 coatings performed comparable to but not better than Al_2O_3 and ZrO_2 in terms of reversible charge capacity and charge transfer resistance increase over long term cycling [82]. As a material of interest for cathode coatings, Titanium Oxide is not as desirable due to its middling nature.

1.7.5.5 CeO_2 coatings

Cerium Oxide is proposed as a good coating for NMC because of its high electronic conductivity compared to other stable oxides, but is relatively unused for this purpose. CeO_2 coated NMC cathodes were prepared by solution method and tested for electrochemical performance [92]. Higher specific capacity and rate performance in addition to EIS studies proved that the very conductive coating enhanced the battery's kinetics. After 12 cycles, charge transfer resistance of uncoated was about five times that of CeO_2 coated cathode. Cycling at high temperature showed that CeO_2 also provided protection against electrolyte side reactions, as high rate cycling of the coated cell lost no capacity after 24 cycles compared to about 10% loss of the uncoated cell capacity. CeO_2 deserves to be directly compared to mainstream oxide coatings such as ZrO_2 and Al_2O_3.

1.7.6 Coating Summary

In summary, many different oxide materials have been used to coat on Lithium ion battery cathodes to improve battery capacity, rate capability, and cell lifetime. For layered structure materials, oxides were initially thought to improve lifetime by inhibiting volume change in the active material but the mechanism is now known to be inhibition of side reactions with electrolyte. Oxides have also been utilized to unlock higher potential cycling in batteries allowing larger capacity with less degradation by

electrolyte reactions. These coatings can allow advantages of layered materials like layered $LiNi_xMn_yCo_{1-x-y}O_2$ in order to allow their innate advantages of rate capability and capacity while circumventing common problems of degradation. As well, coatings have been used to enhance stability of spinel $LiMn_2O_4$ cathode materials and improve rate capability of olivine $LiFePO_4$. Materials such as Al_2O_3, ZrO_2, and MgO layers fabricated by chemical methods typify the coating chemistries applied on different cathode structures on the nano scale.

2. SURFACE MODIFICATION OF $LiNi_{0.5}Mn_{0.3}Co_{0.2}O_2$ CATHODES FOR IMPROVEMENT OF BATTERY PERFORMANCE

2.1 Overview

Amorphous nanoscale coatings of Al_2O_3, $Zr_{0.92}Y_{0.08}O_2$ (YSZ), and CeO_2 were applied on doctor blade film $LiNi_{0.5}Mn_{0.3}Co_{0.2}O_2$ cathodes through pulsed laser deposition (PLD) and assembled into half-cell Lithium ion batteries. The microstructural properties of the coatings were characterized by XRD, SEM and TEM along with composition analysis using EDX and STEM. Most of the films are determined to be around 10 nm in thickness. Battery tests were performed on the three coated cells and an uncoated reference sample. Both the CeO_2 and Al_2O_3 coated cells achieved better capacity and showed improved electrochemical performance by EIS, while the YSZ coated one showed decreased capacity and poorer charge transfer kinetics. A direct correlation between the battery capacity and solid-electrolyte interface resistance is established for all the cells. The results suggest that NMC capacity can be improved through surface modification and the resulted SEI resistance inhibition. Further optimization of YSZ film could lead to improved cell performance. Repeatability between runs is to be tested.

2.2 Introduction

$LiNi_xMn_yCo_{1-x-y}O_2$ (NMC) has been proposed as a next generation Lithium ion battery (LIB) cathode material. Advantages in energy capacity, thermal stability, and cost by mixing the three transition metals in the layered structure have been achieved

[93]. Cobalt is able to stabilize the structure and allow higher capacity due to higher Co-O bond energy while Ni and Mn decrease material cost while maintaining stability. However, challenges with NMC still remain specifically in rate capability due to lowered electrical conductivity compared to some other next generation LIB cathodes. Applications such as hybrid electrical vehicles (HEV) and portable power tools would benefit from this enhanced rate performance by allowing faster charging and higher capacity at higher current rates. Also, opportunities exist in exploiting higher voltage charge/discharge reactions to extract more capacity.

2.2.1 Methods for cathode performance improvement

Currently there are three methods for increasing rate performance of cathode materials: decreasing grain size, substitution of transition metals for Li in the cathode, and grain surface coatings. Decreasing the grain size allows a shorter path for Li ions to travel, with the goal of lowering the diffusion length. Particles of most different cathode materials have been created in the nanoscale range, showing enhanced charge/discharge kinetics; however, a drawback of increased surface area for solid-electrolyte interface (SEI) is present. Increasing the SEI will greatly reduce capacity retention by metal dissolution and other harmful side reactions [94]. The second method is through doping. Two different general goals for metal ion substitution (doping) exist; with one substituting metal sites such as $LiNi_{0.5}Mn_{0.3}Co_{0.2}O_2$ and the other substituting Li sites. Doping of Li-containing cathodes has been performed with many materials in order to improve stability and prevent cathode metal dissolution [95]. When the cathode is discharged, there is a framework of doped ions in the place of Lithium remaining that

prevents phase change and allows better cyclability with more available capacity. The drawback of this method is that it requires sacrificing overall capacity by removing Li ions before any cycling. The third approach is cathode surface coatings. Coating cathode grain particles through chemical or physical methods can increase capacity, rate capability, and capacity retention by several different methods. On nanoscale grains, surface stress between active material and coating has been proposed to enhance structural stability and inhibit phase changes, which would allow higher capacity and allow faster rate cycling [42]. Surface chemistry modification is also proposed as a method for rate capability increase [94]. Capacity retention is achieved by preventing physical cathode-electrolyte contact which can facilitate metal dissolution and also acting as a sink for harmful HF acid. Materials used for coating include Carbon, conductive metals, metal oxides, and polymers. Carbon has been utilized both as a bulk active material-binder solution additive and as thin films applied to each active material grain for purposes of surface modification and electronic conductivity enhancement [80].

2.2.2 Metal oxide cathode surface coatings

Metal oxides are heavily researched with regards to their effects as surface coatings. Research is ongoing in finding more useful oxide coatings and discovering the precise mechanisms for improvement; however, literature results regularly conflict and lack consistency in conclusions. Battery assembly, cathode preparation, and electrical testing methods all vary among published results which can lead to misleading comparisons. Several survey studies of coatings have been done yielding differing and sometimes conflicting results in magnitude and mode of improvements [41; 42; 96].

Al_2O_3 and ZrO_2 coatings are heavily studied across cathode materials for capacity and lifetime enhancement [51; 58; 66; 89; 97]. Yttria stabilized Zirconia (YSZ) is ZrO_2 doped with a small amount of Y_2O_3, and is used in solid oxide fuel cell electrolytes. It displays high ionic conductivity and is very stable chemically, though it does show low electronic conductivity [98]. CeO_2 is an oxide used mainly in catalysts that displays excellent electrical conductivity as a film on other oxides [99] and with this benefit in mind has recently been studied for coating cathodes [63; 77; 92].

2.2.3 Coating methods

Typically a solution or chemical coprecipitation method is employed to apply cathode coatings by weight percent. These methods rely on specific reactions and optimization of reaction temperature, and sometimes suffer from hybrid surfaces (for example, an MgO coating on $LiCoO_2$ might create a $LiMg_xCo_{1-x}O_2$ layer) [53]. Utilization of the precise atomic layer deposition (ALD) technique for coating has resulted in impressive improvements compared to thicker chemical methods[84]. However, ALD is limited in breadth of possible coating materials. Pulsed laser deposition is another precisely controllable method for deposition on cathodes that is not as limited in material selection. Thus, PLD is optimal for creating coatings of precise thickness and varying stoichiometry in order to quickly screen different materials' cathode coating effects. In this study, pulsed laser deposition of oxides Al_2O_3, $Zr_{0.92}Y_{0.08}O_2$, and CeO_2 was applied to composite $LiNi_{0.5}Mn_{0.3}Co_{0.2}O_2$, Carbon, poly-vinylidine fluoride (PVDF) cathodes in order to compare the effects in terms of capacity, rate capability, and capacity retention.

2.3 Experimental Details

2.3.1 Doctor blade deposition of cathode

$LiNi_{0.5}Mn_{0.3}Co_{0.2}O_2$-Carbon-PVDF composite cathode was deposited on Aluminum foil using the doctor blade method. The doctor blade method is used in many different ceramic thin-film processing applications. It involves using a blade to precisely level the thickness of a solution on substrate which then dries into a film. It allows film thickness control on the order of micrometers, though once a film dries it loses thickness and changes morphology based on percentage of solvent/solutes and drying mechanisms. First, commercial NMC, C-45, and PVDF powders were weighed in 10/1/1 weight ratio. N-methyl-2-pyrrolidone (NMP) solvent was heated to 80° C in lead ball-mill container and PVDF was added with steel balls. PVDF was mixed with high-energy ball mill for five minutes to ensure binder uniformity across solvent, and then Carbon and NMC powders were added to ball-mill container. Mixture was high energy ball milled for around three hours to both break down NMC grains below the commercial ~10μm size and also to ensure thorough mixing. Mixed solution was optimized for porosity of resultant film, adhesion to Al foil surface, and electrical performance. Then mixture was spread and leveled at 100 μm on Al foil by doctor blade. Fig. 10 shows the doctor blade spreading/leveling process and a typical resultant spread film.

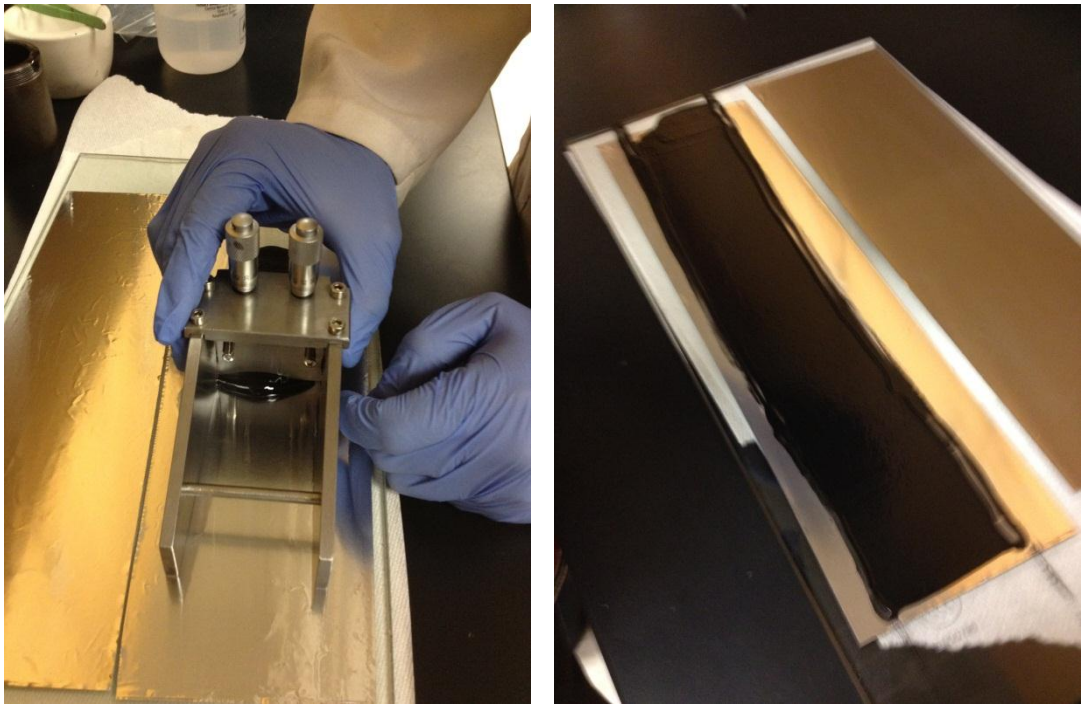

Fig. 10: Doctor blade spreading of composite solution and finished film on Al foil

After spreading, the doctor blade film on Aluminum foil was heated to 90° C on a hot plate to dry the NMP solvent and promote adhesion. Once they were visibly dry and secured from the solution running, smaller sheets were cut and placed into box furnace at 90° C for 24h. Cathodes were cut in 13mm diameter circles by hand punch. Active material (NMC) mass was between 5-6 mg in each cathode. In order to further promote adhesion and electrical contact, film porosity was reduced by pressing for 10 minutes.

2.3.2 Cathode surface coating through pulsed laser deposition

Cathodes were then coated with very thin oxide layers using pulsed laser deposition (PLD). PLD is a physical deposition method whereby a high energy ultraviolet laser strikes a target in vacuum and induces ablation [100]. Vaporized target

material then condenses on the substrate in a manner determined by chamber conditions such as ambient gas choice and gas pressure, substrate temperature, and laser energy density. The laser used for this project was a 248nm KrF excimer laser. PLD carries advantages over other deposition methods such as thermal evaporation or chemical vapor deposition because of its precise control over film stoichiometry, thickness, and crystallinity. It also exhibits a simple experimental setup and broader film material choice compared to other precise deposition methods such as atomic layer deposition. Fig. 11 shows a diagram of a typical PLD system and a picture of Cerium Oxide plasma being deposited on the composite cathodes for this project.

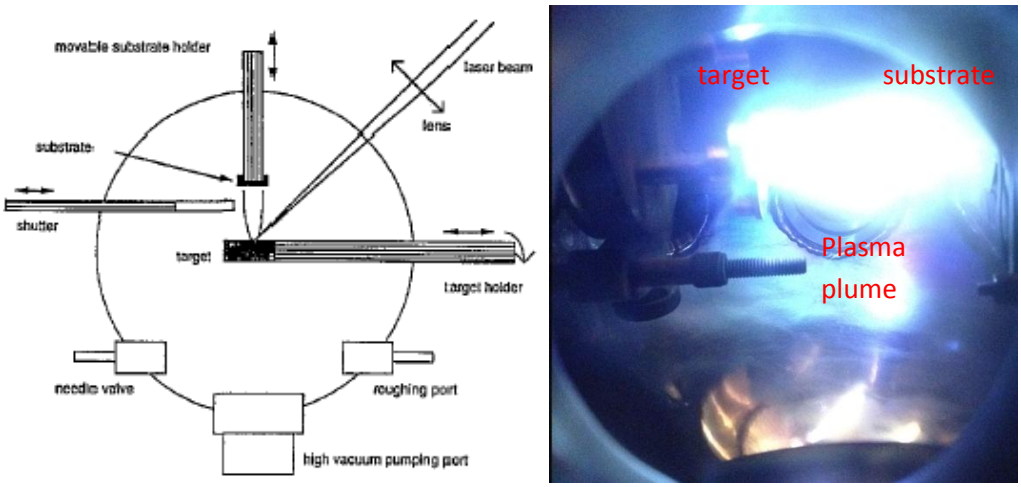

Fig. 11: Schematic of typical PLD chamber[101] and picture of PLD chamber in use

The doctor blade composite cathodes were used as substrates for depositions of Al_2O_3, $Zr_{0.92}Y_{0.08}O_2$ (YSZ), and CeO_2. Alumina was deposited with 200 laser shots at a rate of 1 Hz with 400 mJ energy per shot at room temperature in $1.9*10^{-2}$ mbar (~14

mTorr) of O_2, and Ceria and YSZ were separately deposited with 100 shots under the same conditions. Deposition rates for the YSZ and Al_2O_3 targets were determined by separately depositing thin films with 1000 and 2000 shots, respectively, on Si (100) and measured with a Veeco profilometer. Deposition rate for CeO_2 target under project conditions were known. Targets and films were examined with x-ray diffraction (XRD) to test stoichiometry and crystallinity. Cathodes were characterized with transmission electron microscope (TEM), scanning transmission electron microscope (STEM), and scanning electron microscope (SEM) coupled with energy dispersive x-ray spectroscopy (EDX) for film microstructural characterization and composition analysis.

2.3.3 Battery Assembly

After cathodes were deposited by Doctor Blade method and coated with PLD layers, batteries were assembled in glove box with Argon ambient. Before placing in the glove box, cathodes were placed in the furnace at 90° C to remove moisture. The glove box is necessary for battery assembly to minimize Li foil oxidation in presence of oxygen. As well, the electrolyte solution of ethyl carbonate: diethyl carbonate (EC:DEC) ratio 1:1 with 1M $LiPF_6$ could form HF acid in the presence of moisture. Assembly proceeded by placing cathode in 2032 size coin cell positive casing, face up. Celgard polypropylene film circularly cut 16mm in diameter was placed next as a separator layer, followed by a circle of Li foil 15mm diameter. Finally, two squares of Ni foam were placed above the anode to act as a conductive spacer ensuring electrical contact. Fig. 12 is a picture of all major components in sequence from left to right: positive casing, cathode, separator, anode, Ni foam, and negative casing. The assembled cell was then

crimped by hydraulic crimper to completely seal cell from atmosphere and maintain electrical contact between casings and current collectors/electrodes. The assembled and crimped batteries were made to rest for a day before undergoing electrical tests.

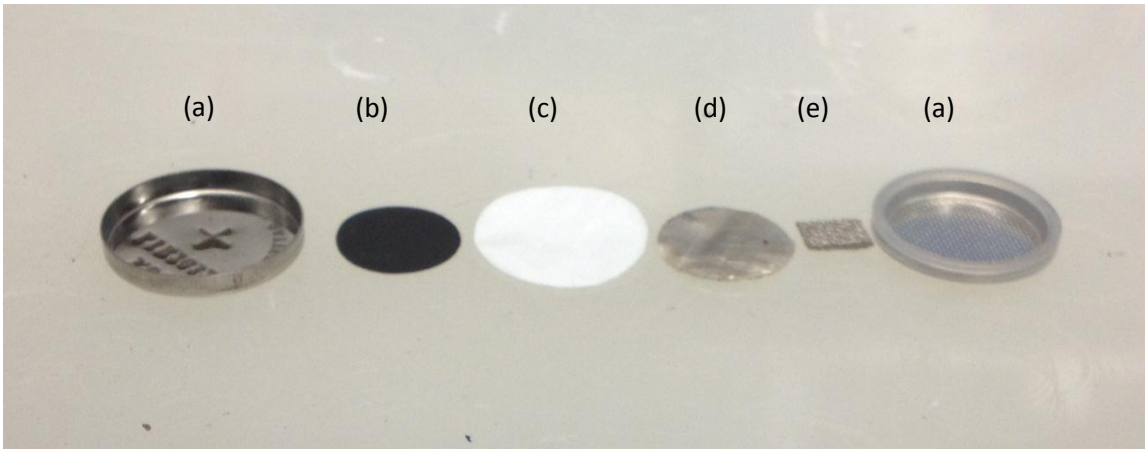

Fig. 12: Coin cell components: (a) casings, (b) cathode, (c) separator, (d) Li anode, and (e) Nickel foam spacers

2.3.4 Electrical Characterization Methods

Electrical characterization by several methods was applied to the assembled batteries. Methods that involve fully cycling the battery include galvanostatic intermittent titration testing (GITT) and cyclic voltammetry (CV). Both GITT and CV tests were performed on uncoated and coated cells with an Arbin BT-2000 battery tester system. GITT involves applying constant current to galvanostatically charge and discharge the battery between predetermined voltages. The total amount of current used to charge or discharge the battery to desired voltage is the charge or discharge capacity. Charge and discharge curves under GITT can reveal many facts about a cathode

including capacity, reaction potentials, and Li diffusion constant. Fig. 13 shows typical discharge curves of NMC under different currents.

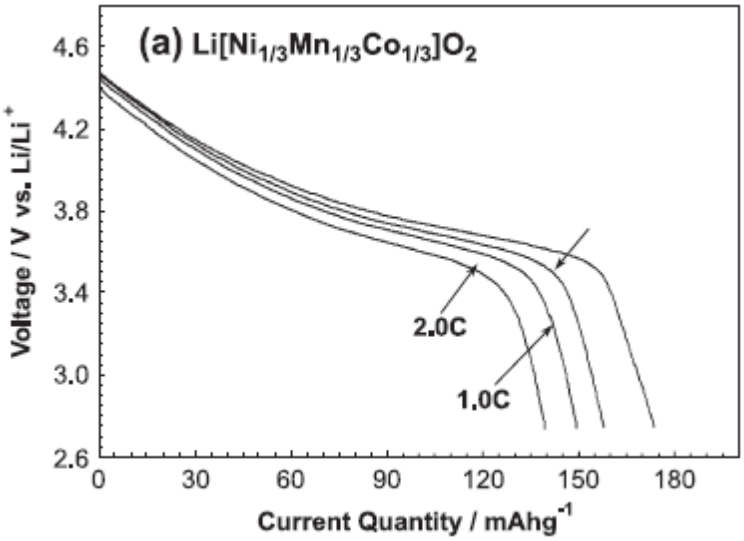

Fig. 13: Typical discharge curves at various rates of NMC battery from literature [102].

The number of hours to charge or discharge is the C-rate, and is measured in terms of battery capacity. Thus, if charged at 1 C a battery will take 1 hour to charge and when discharged at 0.2 C a battery will take 5 hours to discharge. When applying larger currents, less capacity might be achieved due to battery kinetics limiting electrically available regions. An area of low slope, known as a voltage plateau, indicates that much capacity is stored in that potential region which means that there is a reaction at that potential. It is important to note the boundary voltages used for capacity measurements. If a battery is cycled between a larger voltage range (especially above 4 V), it is likely that more capacity will be gained. Much ongoing research in coatings involves enlarging

capacity by broadening the safe voltage range through electrolyte selection or cathode coatings. Galvanostatic cycling is one of the most fundamental electrical tests relied upon to understand battery activity.

In contrast to GITT, cyclic voltammetry (CV) involves voltage control of the battery. CV tests are run by slowly ramping the voltage up and down through the battery's active range to charge and discharge. CV is very similar to GITT in that both input only current or voltage control on the battery and measure the other. CV is also able to determine diffusivity of Li ions given data from several different ramp rates. Fig. 14 shows a typical CV curve of NMC.

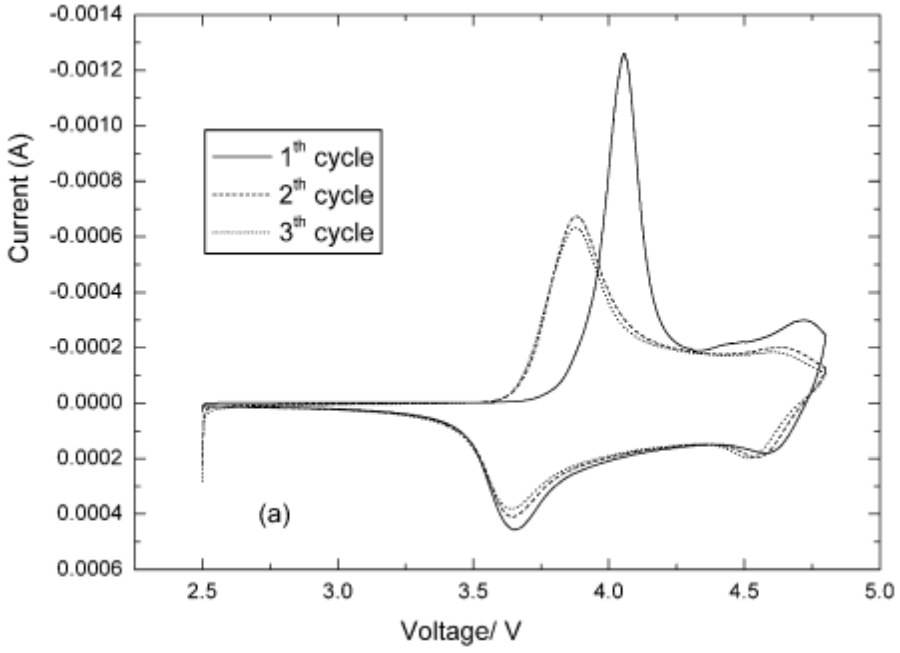

Fig. 14: Cyclic voltammetry curve of NMC battery for first three cycles. Anodic and cathodic peaks indicate main voltages of reaction containing capacity [90].

Resultant current peaks from a CV shows reaction potentials which could indicate phase changes or intercalation potentials. In the case of NMC, peaks of 3.7 V and 4.6 V correspond to the voltages of Ni^{2+}/Ni^{4+} and Co^{3+}/Co^{4+} transitions [90]. The first and second charges have peaks at different potentials indicating a change in chemistry or structure. Such slight changes in peak voltage might be due to increased grain domain polarization or shielding from a solid-electrolyte interface layer [103]. As well, the first peak displays much more current than any subsequent peak due to the nature of SEI formation upon first cycle. Several chemical reactions occur at the cathode-electrolyte and anode-electrolyte interfaces upon the first cycle which results in irrecoverable capacity loss.

Electrochemical impedance spectroscopy (EIS) is a test using alternating current at several different frequencies to probe the electrochemical processes involved in intercalation. It is used to shed light on the physical mechanisms by which batteries function, and can be used in conjunction with GITT or CV curves to provide a comprehensive picture inside. Cells were charged to a certain voltage and then tested through EIS with a Gamry electrochemical potentiostat intermittently throughout cycling. To test with EIS, voltage is ramped above and below the open-circuit cell voltage at several different frequencies (usually between mHz and kHz). The current that results from the small signal voltage stimulus can then be analyzed to give impedance Z. Using the knowledge that impedance is a combination of real and imaginary parts, or $Z = Z' + jZ''$. One can find the real and imaginary components of the complex impedance. This measurement is done at many frequencies, and the resulting data is impedance

magnitude and phase (or real and imaginary components) for the range. With knowledge of the components of Z at many different frequencies, it is possible to create an equivalent circuit to model the processes. Then each component of the equivalent circuit can be compared to a physical process involved in Lithium intercalation. Fig. 15 is the equivalent circuit used in analyzing EIS data.

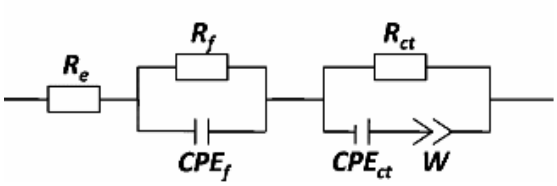

Fig. 15: Equivalent circuit model for battery system including electrolyte, surface film, and charge transfer components [77].

Each circuit component mimics a charge transfer process in the electrochemical battery system. Because these composite cathodes involve nonhomogeneous grain sizes the capacitances have to be modeled with constant phase elements (CPE), which act as $Z_{CPE} = 1/[B(j\omega)^n]$ compared to a normal capacitor's $Z_C = 1/[Cj\omega]$ [84]. R_e is solution resistance, whereby Li ions diffuse and drift throughout the electrolyte solution based on its transport properties. C_f and R_f are surface film resistance and capacitance, which involve the charge transfer process between the active material surface and the electrolyte. C_{ct} and R_{ct} are double layer capacitance and charge transfer resistance, and Z_w is Warburg impedance. The Warburg impedance results from bulk diffusion inside individual NMC grains, and is mathematically represented with $Zw = R_{ct}\sigma(1-j)\omega^{-1/2}$.

Warburg impedance affects total impedance at low frequencies because it relies on intragrain diffusion. The relation between real and imaginary components of the impedance in the system and the equivalent circuit are analogous, and can be represented in a Cole-Cole plot at all frequencies. Fig. 16 shows an annotated Cole-Cole plot of an uncoated NMC cell.

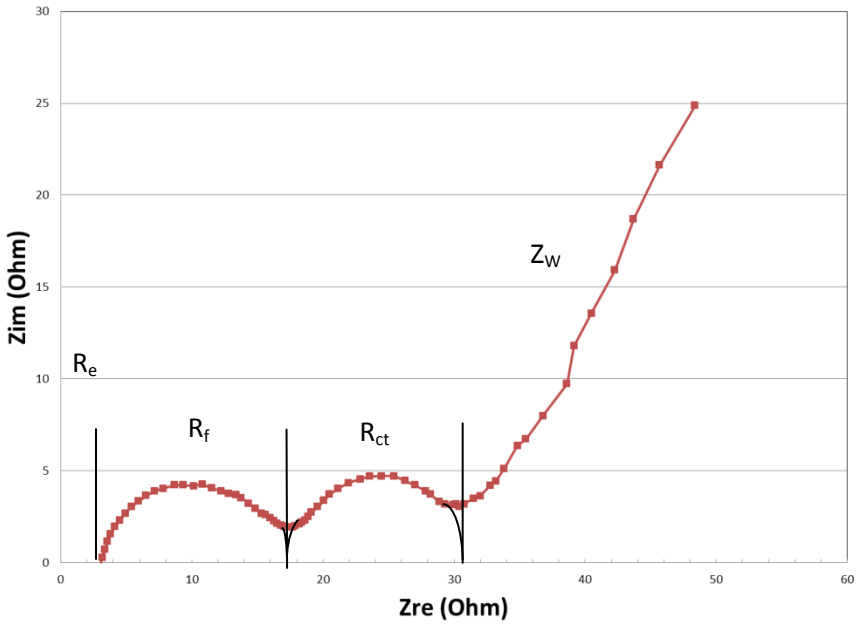

Fig. 16: EIS Cole-Cole plot of uncoated NMC cell marking positions of electrolyte, surface film, and charge transfer resistances [104].

The Cole-Cole plot plots real vs. negative imaginary impedance (because capacitive elements display negative imaginary impedance) and each data point is measured at a different frequency. The beginning of the plot where the curve intercepts the x-axis is R_e, or the pure resistance from solvent of electrolyte and series resistance of the testing setup. This resistance is obviously present in all measurements regardless of

frequency so that is why it manifests as a horizontal shift of the curve. A large R_e might be indicative of poor electrolyte mixing or insufficient contact with testing setup or internally with conductive spacing foam. The diameter of a semicircle corresponding to a charge transfer process mathematically represents its resistance, so R_{ct} and R_f can be quickly derived from Cole-Cole plots for use in characterization. Typically both semicircles are distinct in frequency regions; however, they can become overlapped if the time constants of reaction come within a few orders of magnitude. Finally, the plot ends with the Warburg element with its linear nature implying that slower and slower cycling probes deeper and deeper into each grain.

2.4 Microstructural Characterization

2.4.1 Surface morphology and film thickness characterized by scanning electron microscopy

The cathode by the doctor blade method without a PLD coating was examined using scanning electron microscopy (SEM). The results show a typical morphology of the optimized composition and processing. Fig. 17 shows a plan-view SEM image of a typical doctor blade NMC-C-PVDF cathode on Al foil. The film is composed of NMC grains around 1 μm and below in diameter. This proves that high energy ball milling did break down commercial particles into smaller grains, which should enhance rate performance due to reduced diffusion lengths. The active material in the film seems regularly dispersed within the Carbon/PVDF matrix, showing a highly optimized film.

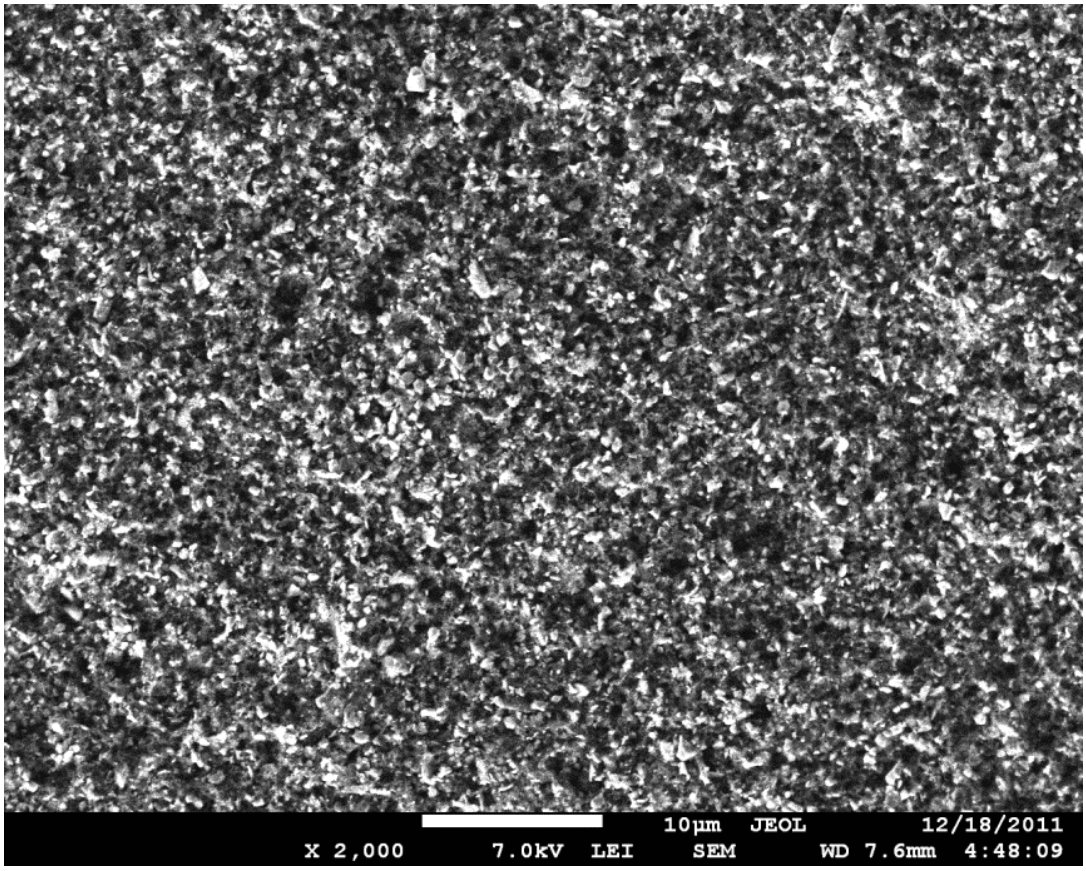

Fig. 17: Plan view SEM image of uncoated NMC-C-PVDF morphology

Fig. 18 shows a cross section SEM image of the Aluminum foil on top and doctor blade film on bottom. From the cross section image, final doctor blade film thickness is roughly 40-50 µm. The blade was set to 100 µm upon solution casting so drying reduced 50-60% of the thickness. The cathode's adherence to Aluminum foil is also visible in the cross section image, and again proves that the process provides good electrical and physical contact to the current collector.

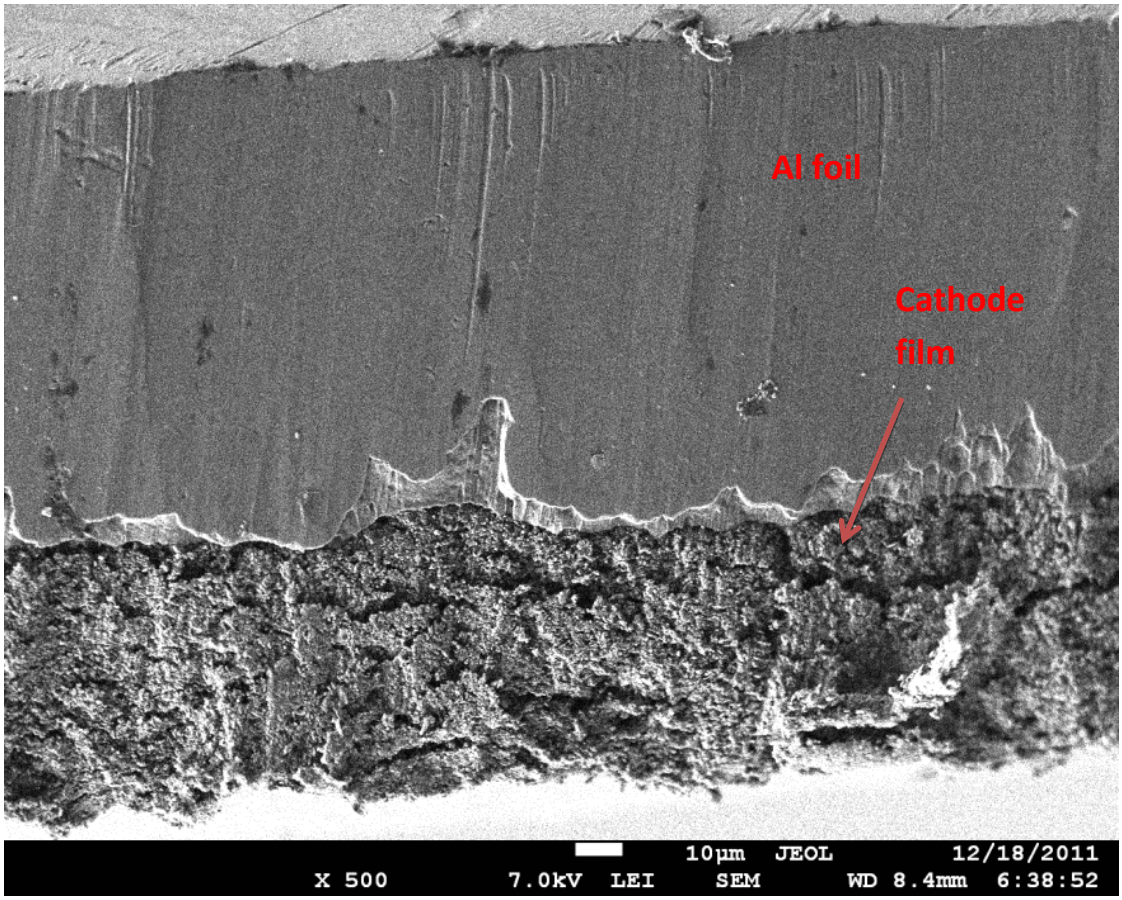

Fig. 18: Cross section SEM image showing NMC-C-PVDF film thickness

2.4.2 Coating verification through energy dispersive x-ray spectroscopy on SEM

In addition to film imaging, both uncoated and Al_2O_3 coated cathode samples were examined in SEM coupled with energy dispersive X-ray (EDX) spectroscopic analysis. The data was compared to verify coating microstructural properties. Fig. 19 shows EDX spectrum of uncoated sample along with elemental identification and associated line scan image. Aluminum is absent in the element identification and line scan only showed background (noise) levels, indicating the sample is free of Al_2O_3 or

any other Al source as expected. Other elements present include Nickel, Manganese, Cobalt, Oxygen, and Carbon all as expected in the composite NMC-C-PVDF cathode. Lithium is too light an element to be viewed through EDX, as not enough electron shells are filled to release viewable characteristic x-rays. Fig. 20 shows the same test completed on an Al_2O_3 coated cathode. Elemental identification reveals Aluminum present in the sum of the line scan, so the coating presence is verified, but resolution of the SEM imaging coupled with vibration do not allow a precise thickness measurement of the coating.

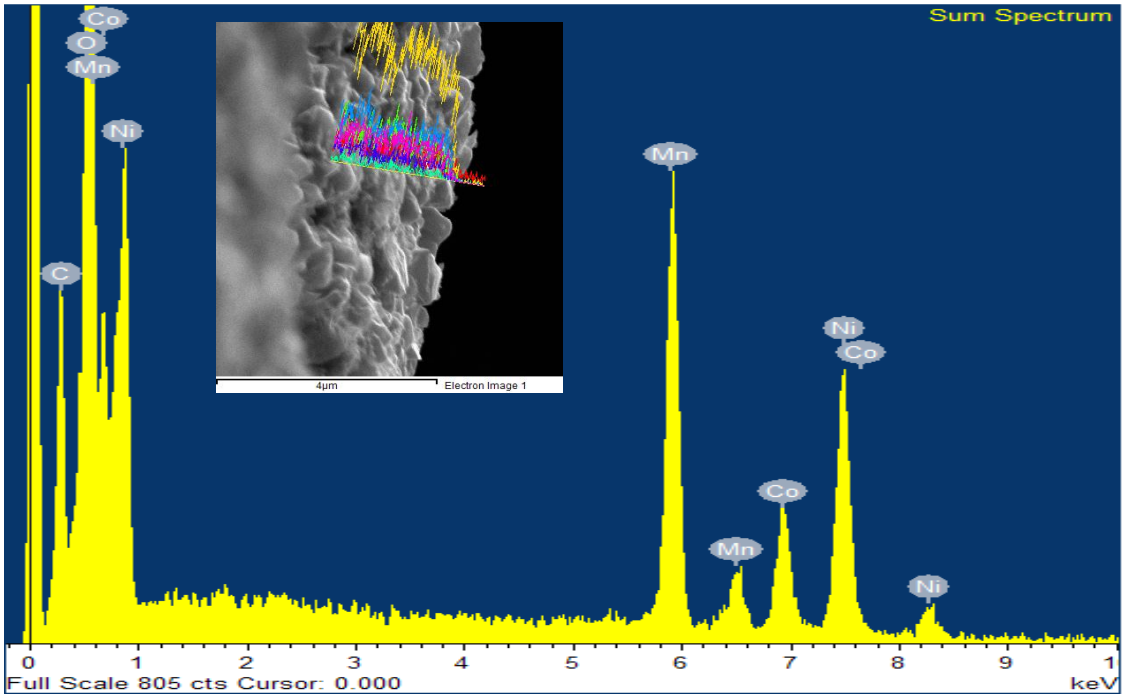

Fig. 19: SEM image with line scan location and EDX energy measurement for uncoated composite cathode.

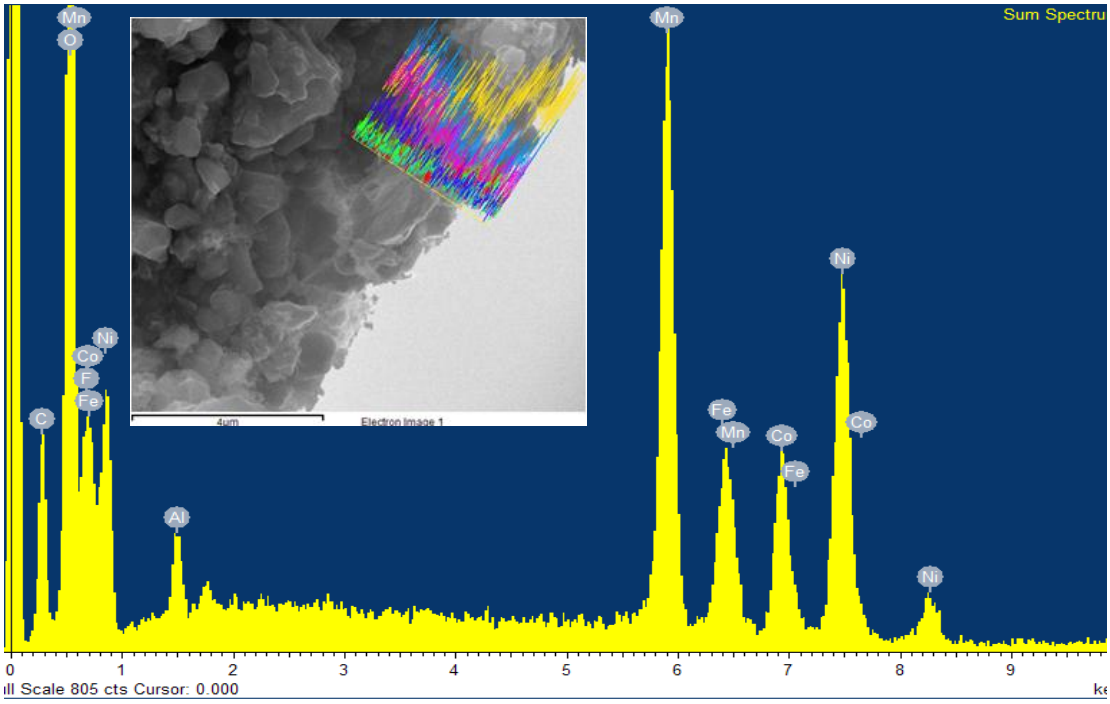

Fig. 20: SEM image with line scan location and EDX energy measurement for Al_2O_3-coated composite cathode. Note presence of Al peak around 1.5 keV.

2.4.3 Microstructure and grain analysis through transmission electron microscopy

Transmission electron microscopy (TEM) was also applied to different samples of uncoated and CeO_2-coated cathodes. Fig. 21 shows a TEM image of singular NMC grains in the conductive matrix of Carbon and PVDF.

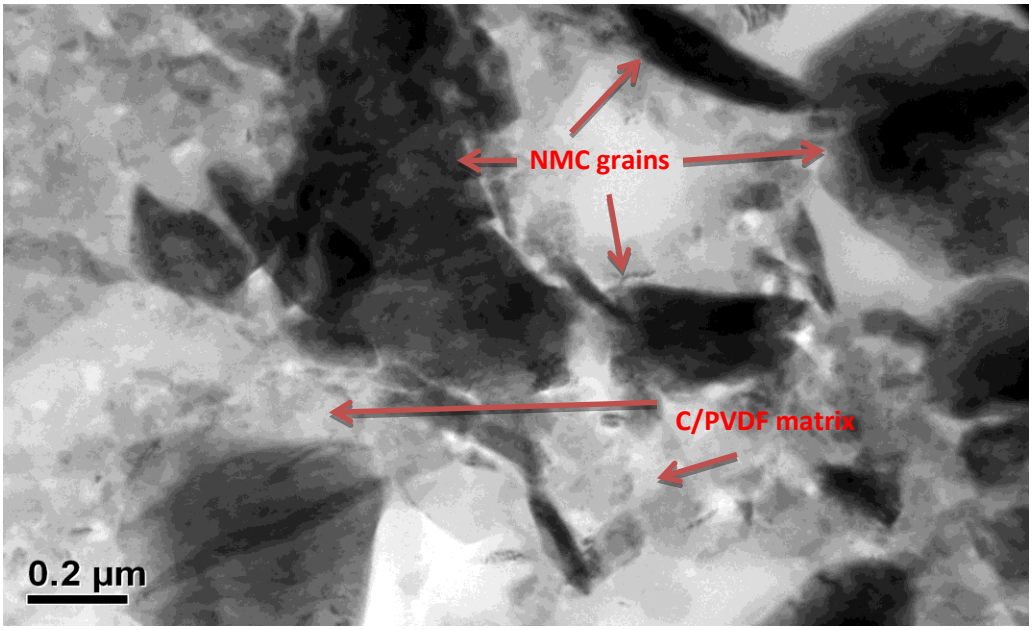

Fig. 21: TEM image of composite NMC-C-PVDF cathode grain morphology. NMC grain size ranges between 0.1 and 0.5 µm.

NMC grains are visible as darker areas, because the metals' heavy atomic numbers diffract/scatter more electrons leaving less transmitted signal. The NMC grain size is clearly observed, suggesting that high energy ball milling has indeed broken up the larger grains into particles between 100-500 nm. As well, it is evident that in order for grain-to-grain conduction to occur, it must be through the C-PVDF matrix that bonds them together. This could be important if this conductive binder is chemically corroded at higher potentials due to the electrolyte's instability. The high volume percentage of C/PVDF versus NMC means that active material grains are basically floating in a conductive matrix. Because the ratio is also present on the surface of the doctor blade film, it means a PLD coating would be applied on both active material and binder. This

could be beneficial to the battery as it could prevent dissolution of the conductive binder thus preserving grain-grain conductivity.

2.4.4 Coating verification through energy dispersive x-ray spectroscopy on STEM

Using scanning transmission electron microscopy (STEM) coupled with EDX, surface grains of NMC coated with CeO_2 were probed for verification of coating. STEM in high annular dark field mode is also called Z-contrast where the image contrast is proportional to Z^2 (more precisely $Z^{1.7}$), i.e., the heavier element shows a brighter contrast. Thus, the brighter material in the image is NMC coated with CeO_2, and medium brightness indicates the C-PVDF binder. Figs. 22 and 23 show the STEM line scan location and EDX elemental identification results of the CeO_2 coated sample, respectively. The green line in the STEM image is the line scanned with EDX. EDX results suggest the existence of the CeO_2 coating, though again coating thickness measurement was made impossible due to the rotations of grains with respect to the axis of measurement.

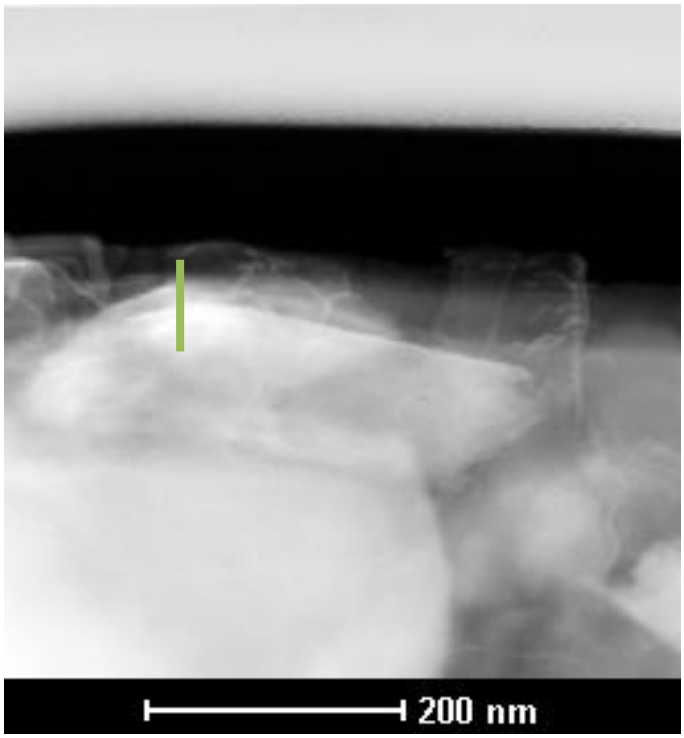

Fig. 22: STEM image of NMC grain and green line showing EDX line scan location.

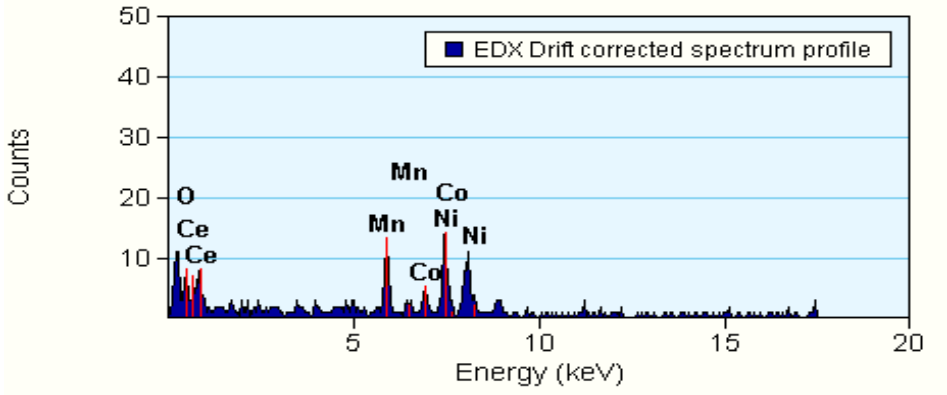

Fig. 23: Energy dispersive x-ray elemental spectrograph of CeO_2 coated cathode showing presence of Ce on grain surface.

Film thickness was estimated based on the growth rate of the PLD method. Under deposition conditions of 400 mJ and $1.9*10^{-2}$ mbar O_2 pressure, the CeO_2 target was known to deposit around 10 Angstroms per shot. Thus CeO_2 film thickness on the cathode is estimated to be around 10 nm, thin enough to improve electrochemical performance as well as act as a chemical barrier.

In order to determine Al_2O_3 and YSZ film thicknesses, test PLD runs of 2000 and 1000 shots respectively on Si(100) using project conditions were performed and film thickness was measured using a profilometer. Al_2O_3 thickness was measured between 75-85 nm, giving a 7.5-8.5 nm coating on the cathode. The measured YSZ film thickness of 80 nm extrapolates to an 8 nm coating on the cathode. All of the coatings are ultra thin and suitable for chemical protection while not expected to inhibit electrical or ionic conduction.

2.5 Electrical Characterization Results and Discussion

2.5.1 Cyclic voltammetry study of reaction potential

Electrical characterization was conducted to show the battery performance differences between the cathodes with and without the select oxides. First, cyclic voltammetry was employed to verify that battery chemistry produced similar reactions. Fig. 24 shows the CV curves of uncoated and two coated cells without any cycling. All CV measurements were ramped at 50 μV/s. Ramp rate could affect the amount of current and the peak position, so it was chosen to be comparable to previous literature reports and slow enough to accommodate battery tester current range.

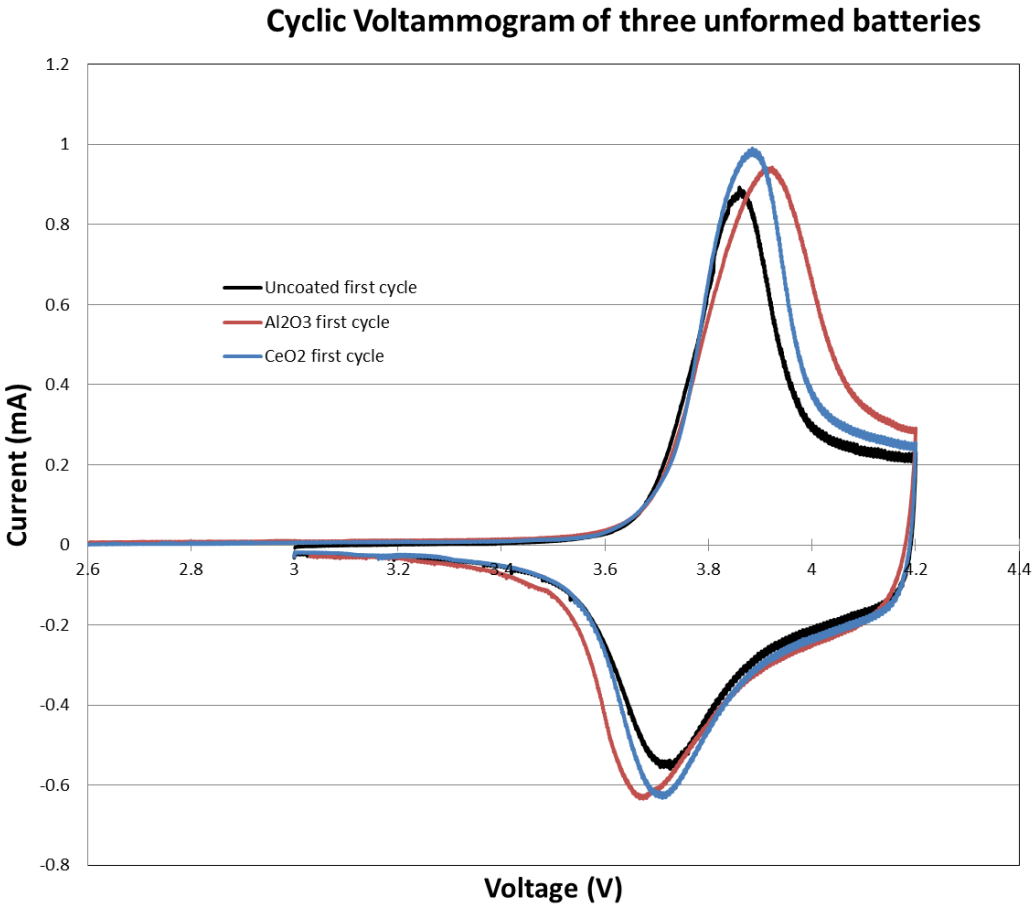

Fig. 24: Cyclic voltammogram of uncoated, Al_2O_3 coated, and CeO_2 coated batteries without any cycling

During voltage ramp up from the starting OCV below 3V to the ending voltage of 4.2 V the battery is charging as seen by the positive current. Lithium is being extracted from the NMC and deposited on Li anode. Then the battery voltage is ramped down to 3V and negative voltage shows it is discharging by Li ions reintercalating into the cathode. Cathodic peaks show slight shifts to more positive voltage, indicating a slightly increased resistance from the coating. Anodic peaks also display a shift in the

opposite direction from the same effect. However, the coating clearly did not affect the chemistry of battery operation as CV shape and peak location remains very similar. Comparing multiple CV cycles between coated and uncoated samples would potentially prove illuminating with regards to reaction peak position and current densities and how the solid electrolyte interface resistance is affected by coating.

2.5.2 Rate capability as a function of cathode surface coating

Fresh coated and uncoated cells were used in order to test rate capability and electrochemical performance. Cells were put through five charge/discharge cycles at 0.2 C, five cycles at 0.5 C, ten cycles at 1 C, ten cycles at 2 C, and ten cycles at 4 C all with respect to theoretical NMC capacity. Cycling was done between 3 V and 4.2 V to include the main Ni^{2+}/Ni^{4+} peak without rising above the electrolyte's stability window. EIS tests were performed on all fully charged cells after first, eleventh, and 41^{st} charge. The goal was to see a difference in EIS (specifically surface film or charge transfer resistance) that was corroborated by a difference in normalized capacity or capacity retention. Afterwards, cells were cycled at 0.5 C between 3 V and 4.6 V in order to test long term high voltage capacity retention. EIS was again taken after 70 and 100 cycles upon charge. This first section will study the evolution of surface film and charge transfer resistance terms extracted from EIS and compare to capacity achieved through galvanostatic cycling. Fig. 25 shows a Cole-Cole plot of EIS data measured after the first charge.

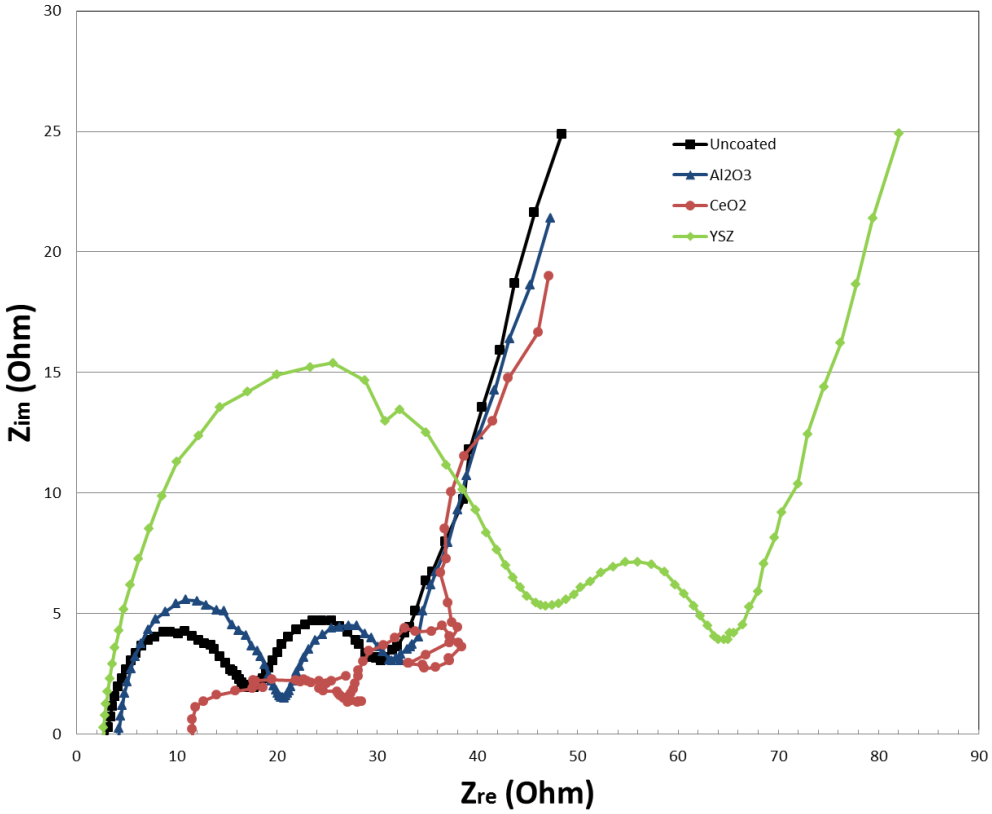

Fig. 25: Cole-Cole plot of all 4 batteries upon first charge at 4.2 V. Electrolyte, surface film, and charge transfer resistances associated with these data are tabulated in Table 3.

Obvious features of the EIS plots are the giant YSZ curve compared to others, and also the noncircular nature of the CeO_2 curve. Throughout all EIS measurements, YSZ consistently showed the largest surface film resistance by more than doubling all other samples' values; however, charge transfer resistance is comparable to uncoated values. This is contrary to some reports, as YSZ has been predicted to enhance battery kinetics similar to that of the regular ZrO_2 [59; 88]. The CeO_2 measurement is noisy which was later determined to be due to poor electrical connection with the EIS probe clamps. This is evident in the increased series resistance with this cell as well as the

nonideal semicircles. However, later measurements were not affected by this noise and estimation of equivalent circuit components upon first charge was still possible. Fig. 26 shows the Cole-Cole plot after 10 cycles. Surface film and charge transfer resistances were estimated using the equivalent circuit in Fig. 15, and summarized in Table 3 for the first and tenth charge. Given the vast range of R_{sf} and R_{ct} from literature due to differences in doctor blade film quality or assembly procedures, it is impossible to predict battery performance directly from the first charge kinetic performance. Instead, one must use self-consistent data throughout battery lifetime to view the evolution of the battery and infer SEI growth and other processes from the results.

Initially, surface film and charge transfer resistances for the cells are of comparable magnitude except for the YSZ coated cell which has R_{ct} about twice of R_{sf}. This similarity between the coated and uncoated values implies that the initial formation charge does not create much SEI on any samples or that the amount is comparable with the coated samples. After ten cycles, surface film resistance stays mostly constant although the CeO_2 sample actually decreased in value while all other samples slightly increased. After ten cycles the kinetics of the CeO_2 cell surface film charge transfer processes have improved or at least stayed the same within margin of error, which is the first sign of improvement. Charge transfer resistance of uncoated and YSZ coated cells more than doubles after 10 cycles, while Al_2O_3 and CeO_2 cells increases to a lesser amount. At this point, R_{ct} seems to be growing slightly more than R_{sf} in all cells, implying that electrical contact between grains is affected more by slow, low-voltage cycling than electrical processes at the cathode-electrolyte layer. Further, this effect is

more prominent in the non-optimized YSZ coated and uncoated cells. This might be due to the normal electrolyte dissolution of binder or the degradation of current collector.

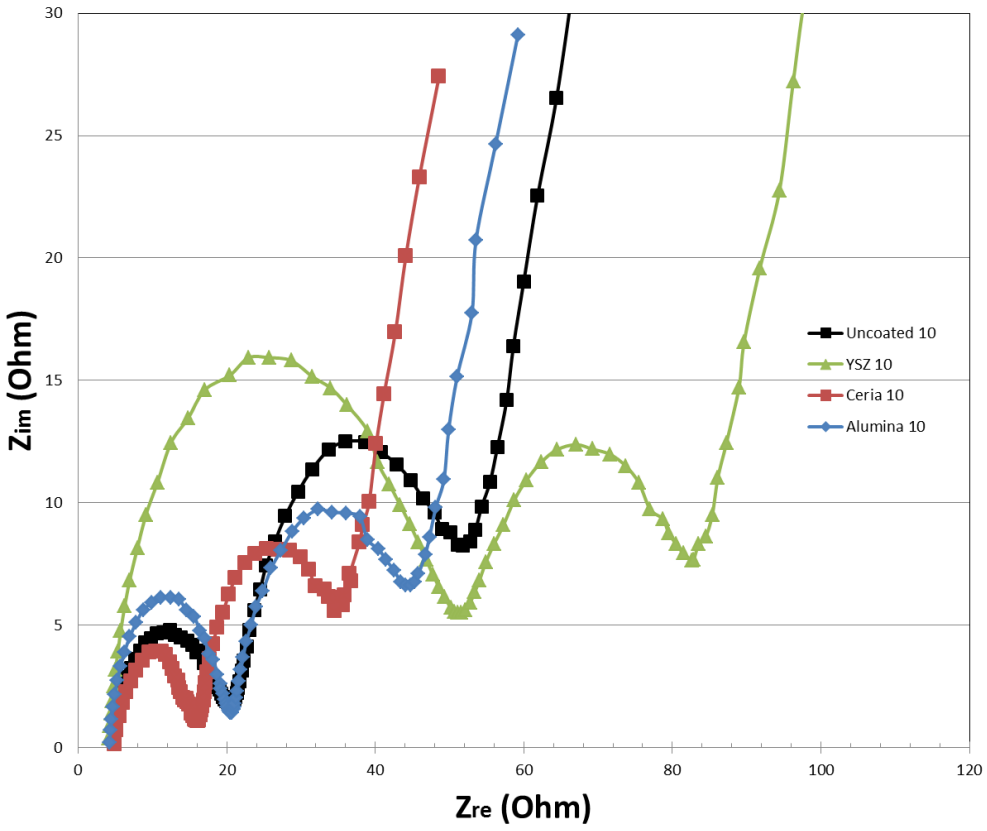

Fig. 26: EIS spectrum after 10 cycles. The trend between cells' surface film resistances continues while uncoated and YSZ coated cells increase much more in charge transfer resistance.

Table 3: Electrochemical properties of cells throughout cycling

	Uncoated	Al_2O_3	CeO_2	YSZ
R_{sf} 1 (Ohm)	15	16	15	44
R_{ct} 1 (Ohm)	14	11	12	18
R_{sf} 10 (Ohm)	16	17	12	50
R_{ct} 10 (Ohm)	**40**	27	22	**40**

2.5.3 Galvanostatic charge/discharge curve analysis

Charge/discharge plots of all cells for the first cycle are shown in Fig. 27. First charge capacities are usually ignored because during this process there is irreversible capacity loss at several different locations, with the most importance for this work being the formation of SEI on the cathode/electrolyte surface.

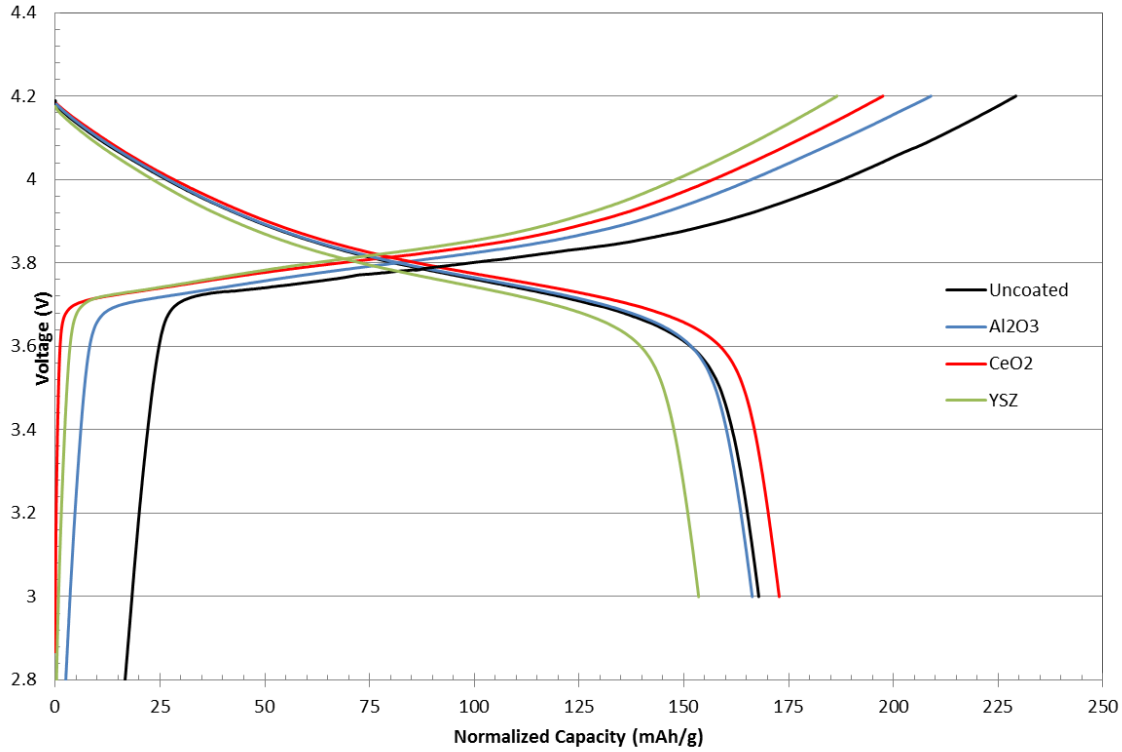

Fig. 27: First charge and discharge cycle for all cells. Charge capacities are not representative due to resulting formation of surface SEI films. Discharge capacities closely resemble the first charge EIS results.

Though the uncoated sample contains the largest charge capacity at the first charge, this is lost and the CeO_2 coated cell has the largest discharge capacity of 172.8 mAh/g (compared to 167.9 mAh/g for uncoated, 166.3 mAh/g for Al_2O_3 coated, and 153.5 mAh/g for YSZ coated). Capacity retention between the first charge and discharge is the amount of capacity lost to irreversible processes, which can be an estimation of SEI-associated loss. In that regard, again the CeO_2 cell surpasses the others with a retention percentage of 81.3% (compared to 71.0% for uncoated, 77.7% for Al_2O_3 coated, and 79.4% for YSZ coated).

Typical discharge curves throughout battery cycling are shown in Fig. 28. Different capacities are achieved due to different cycling rates being applied and also electrochemical processes occurring inside the battery degrading performance. One of these sources of reversible capacity loss is grain domain polarization which in the equivalent circuit model acts as a series resistance in the cell 'stealing' voltage from the reaction [53]. This can be seen in the initial voltage drop difference between different discharge rates. A larger discharge current could drop more voltage across a series resistance thus starting off at a lower voltage, which can easily be seen in the figure. The change in slope of the discharge curve throughout cycling also shows electrochemical differences between initial and high rate cycling. A completely flat voltage plateau in charge or discharge cycles indicates a solid solution between lithiated and delithiated phases at the potential at which a reaction occurs; therefore, if it becomes less flat the reaction is distributed in a two phase system [71]. This means lithiation of the cathode (upon discharge) might be hindered or electrically screened by a coexisting lithiated phase in the same grain. This can also be explained through the grain polarization mechanism.

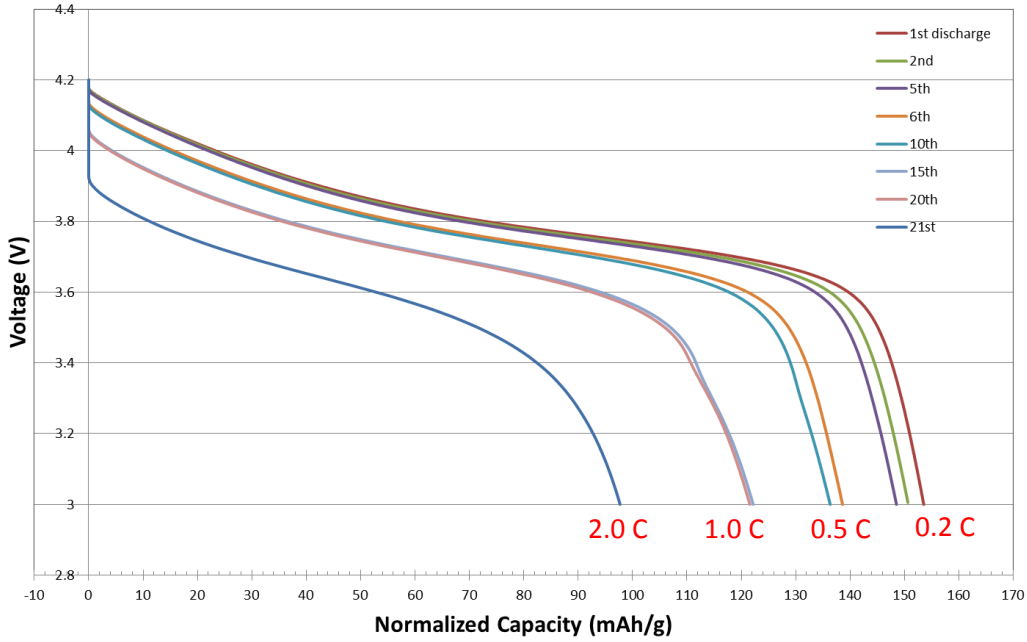

Fig. 28: Discharge cycles for several different rates. Increasing discharge rate causes increased polarization and reversibly diminished capacity. As well, capacity is slowly lost throughout cycles at the same rate especially in first cycles.

Finally, the rate capability of all batteries was examined and compared between 0.2 C and 4 C. The normalized capacity of each cell for each cycle is shown in Fig. 29. Fig. 30 shows the percentage of capacity retention at each rate compared to initial capacity for each cell. Capacity retention percentage was calculated by averaging discharge capacity for all cycles at each rate because no cycle-to-cycle degradation was visible. CeO_2 performed the best which is consistent with its kinetic performance in EIS tests, and YSZ performed the worst, also seen in EIS tests. It is believed that CeO_2 performed the best due to its beneficial electrical conductivity compared to other coatings as well as its chemical inertness [99]. Conversely, YSZ is structurally very similar to simple ZrO_2 which has been known to enhance capacity and kinetics, so the

poor performance in rate capability and flat capacity is still not yet clear. The YSZ coating is so thin that it is unlikely to be a thickness/conductivity optimization problem. As well, the natural polarizability of oxygen vacancy complexes in YSZ could be the reason for poor EIS and electrical testing results. Repeatability tests should be done to clarify where this effect came from.

Al_2O_3 performs remarkably similarly to the uncoated cell at low rates, and at higher rates actually surpasses uncoated performance. Al_2O_3 has been extensively studied as a surface coating for cathode materials, and it is well known that Al_2O_3 has the effect of inhibiting SEI formation [81]. This in turn prevents capacity degradation and is evident in EIS after cycling. Its thin coating here seems to have not inhibited the battery kinetics compared to an uncoated battery, and the benefits become evident in increased capacity once many cycles have taken place (several days of real time). However, the surface film resistance of Alumina and uncoated cells are comparable and actually the charge transfer resistance is where Al_2O_3 coating seems to slightly improve the performance. The mechanism for the enhancement here is still under investigation. One possible mechanism is that the coating is applied to carbon and binder on the surface and strengthens these components from electrolyte dissolution, thus preserve grain to grain conduction. However, more study is needed of coatings' effects on charge transfer resistance evolution.

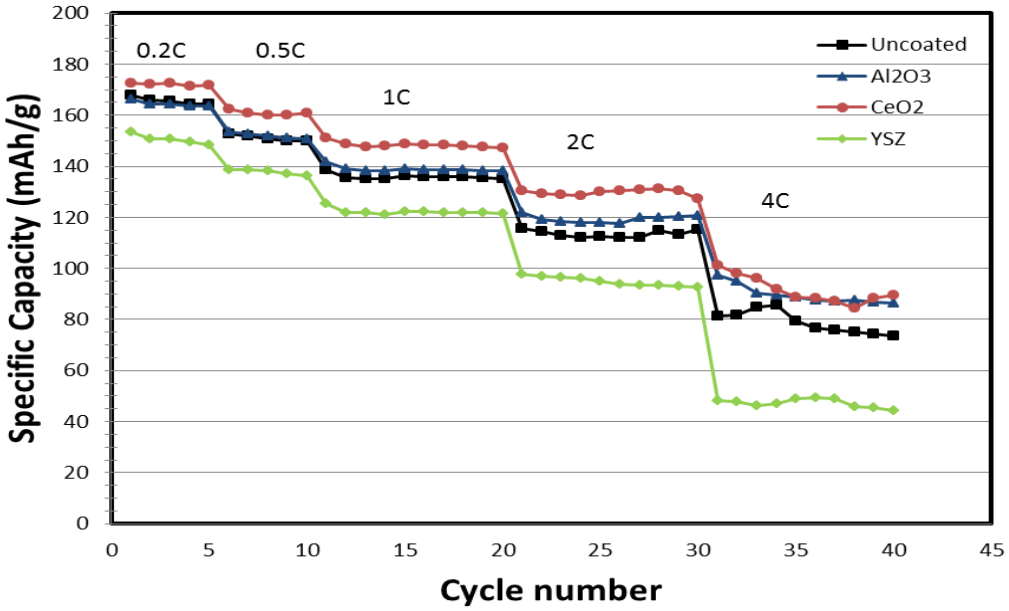

Fig. 29: Rate capability of cells between 0.2 C and 4 C. CeO_2 performs the best at all rates, and Al_2O_3 improves throughout testing compared to uncoated cell. YSZ consistently underperforms compared to uncoated cell.

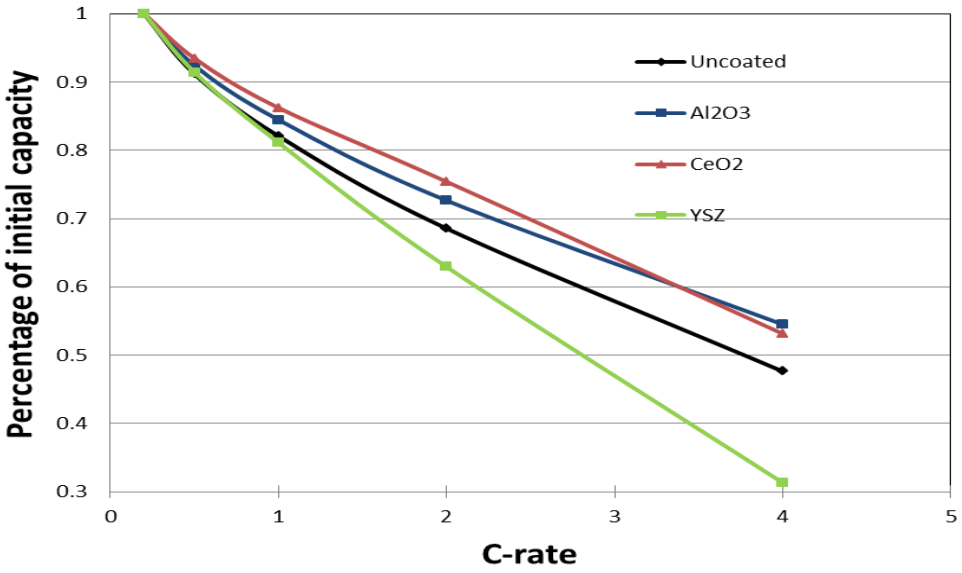

Fig. 30: Percent capacity retained at each rate. Again CeO_2 coating and Al_2O_3 coatings see increased rate performance compared to uncoated cell due to enhanced battery kinetics.

2.5.4 High voltage performance

After testing rate capabilities, the battery was cycled between 2.8 V and 4.6 V at the rate of 0.5 C. During this cycling, cells were tested with EIS after 40 and 100 cycles. The motivation behind this test is that coatings are expected to inhibit harmful reactions between electrolyte and active material that occur at higher voltages, thus maintain the cell capacity. Fig. 31 shows a comparison of CV curves when cycled between 3-4.2 V and 3-4.6 V. The second battery cycle was used to ramp to 4.6 V, so the loss of capacity in the peaks is explained by the irreversible loss associated with formation cycling. The area under the curve between 4.2 V and 4.6 V is the significant extra capacity obtainable by cycling in the higher voltage region. This shows why it is so advantageous to find ways to utilize charge and discharge in higher voltages with this battery chemistry.

First charge and discharge plots at high voltage for all cells are shown in Fig. 32. The capacity performance hierarchy is similar to the first test, with the exception that the Al_2O_3 coated cell now slightly outperforms the uncoated. As explained before, this is probably due to the Alumina coating's ability to inhibit dissolution of conductive matrix which normally can cause drastic increases in charge transfer resistance. Also of note in the high voltage region is that there exists no extra voltage plateau around 4.5 V, whereas one has been predicted to correspond with the Co^{3+}/Co^{4+} reaction [105]. Instead, the slope continues almost unchanged which suggests a continuously distributed reaction. If cells were initially cycled at the elevated voltage, the plateau might be found from the pristine state. The discharge capacities are larger than charge capacities because previous cycles caused so much polarization that cells were never truly discharged to 3.0

V. Thus, the charging starts around 3.75 V, and the lower voltage charge peak and associated capacity are missing.

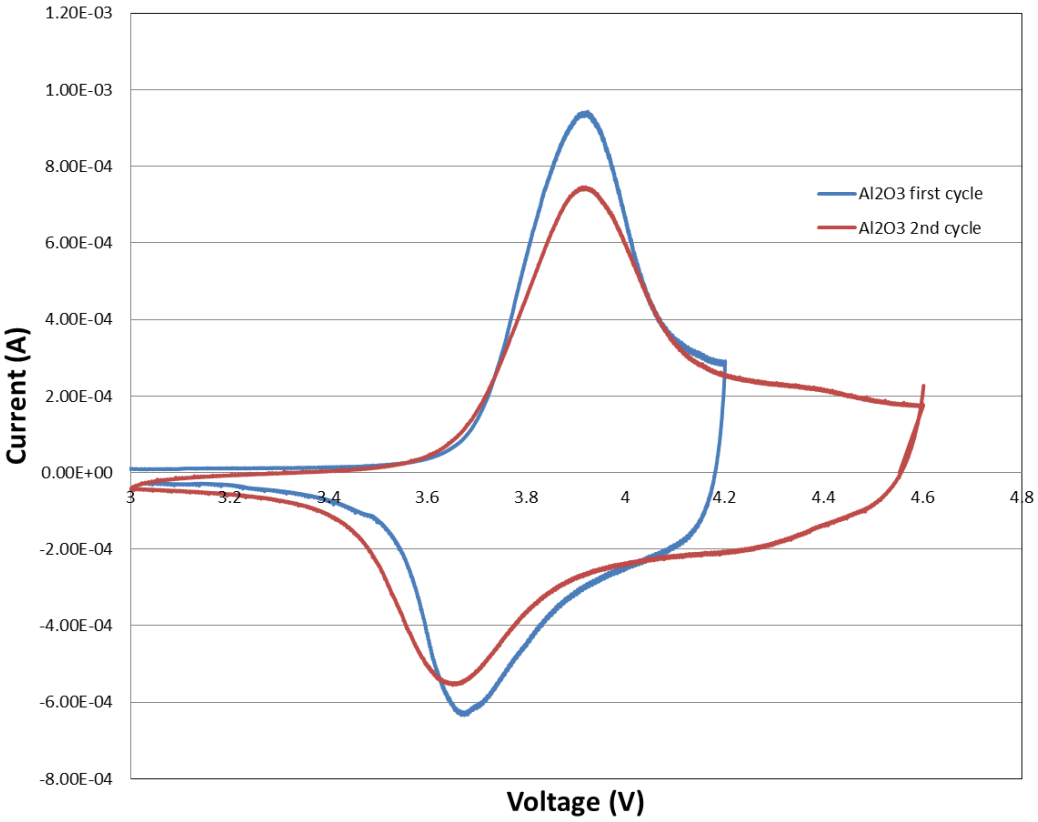

Fig. 31: Cyclic voltammetry curves between 3-4.2 V (blue) and 3-4.6 V (red). Area under the red curve is increased capacity due to cycling at higher, potentially damaging voltage.

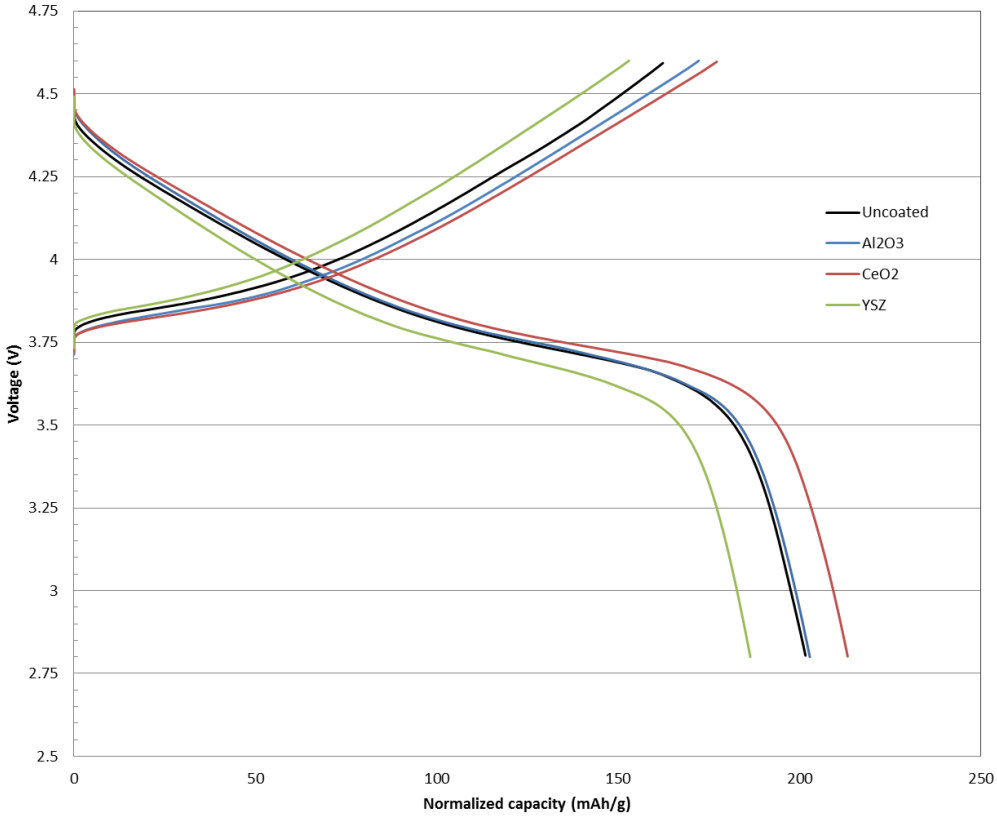

Fig. 32: First charge and discharge for all cells at high voltage. The capacity trends the same as lower voltage, and there are no voltage plateaus indicating a phase change in the high voltage region.

During high voltage cycling, EIS was again employed to probe the electrochemical performance of each cell. Fig. 33 shows EIS Cole-Cole plot before high voltage cycling (after 40 cycles), Fig. 34 shows EIS Cole-Cole plot after the 60 high voltage cycles and 40 initial cycles, and Table 4 tabulates the surface film and charge transfer resistances of each cell. Changes in solution/series resistance are negligible compared to other values and so are not noted. After 40 cycles, but before high voltage cycling the CeO_2 cell has the smallest surface film and charge transfer resistances, and the YSZ cell has the largest. At this point the degree of frequency overlap in the separate

components is the most in the YSZ coated cell, implying that the surface film process is slowed to near the order of the intergrain charge transfer process.

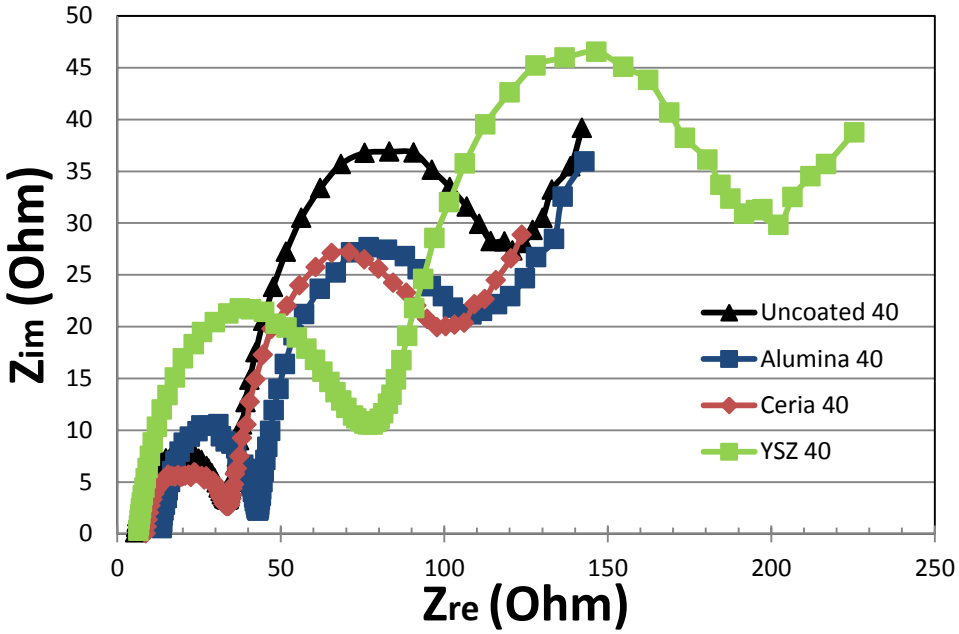

Fig. 33: EIS spectrum before high voltage cycling. Electrolyte, surface film, and charge transfer resistances are tabulated in Table 4.

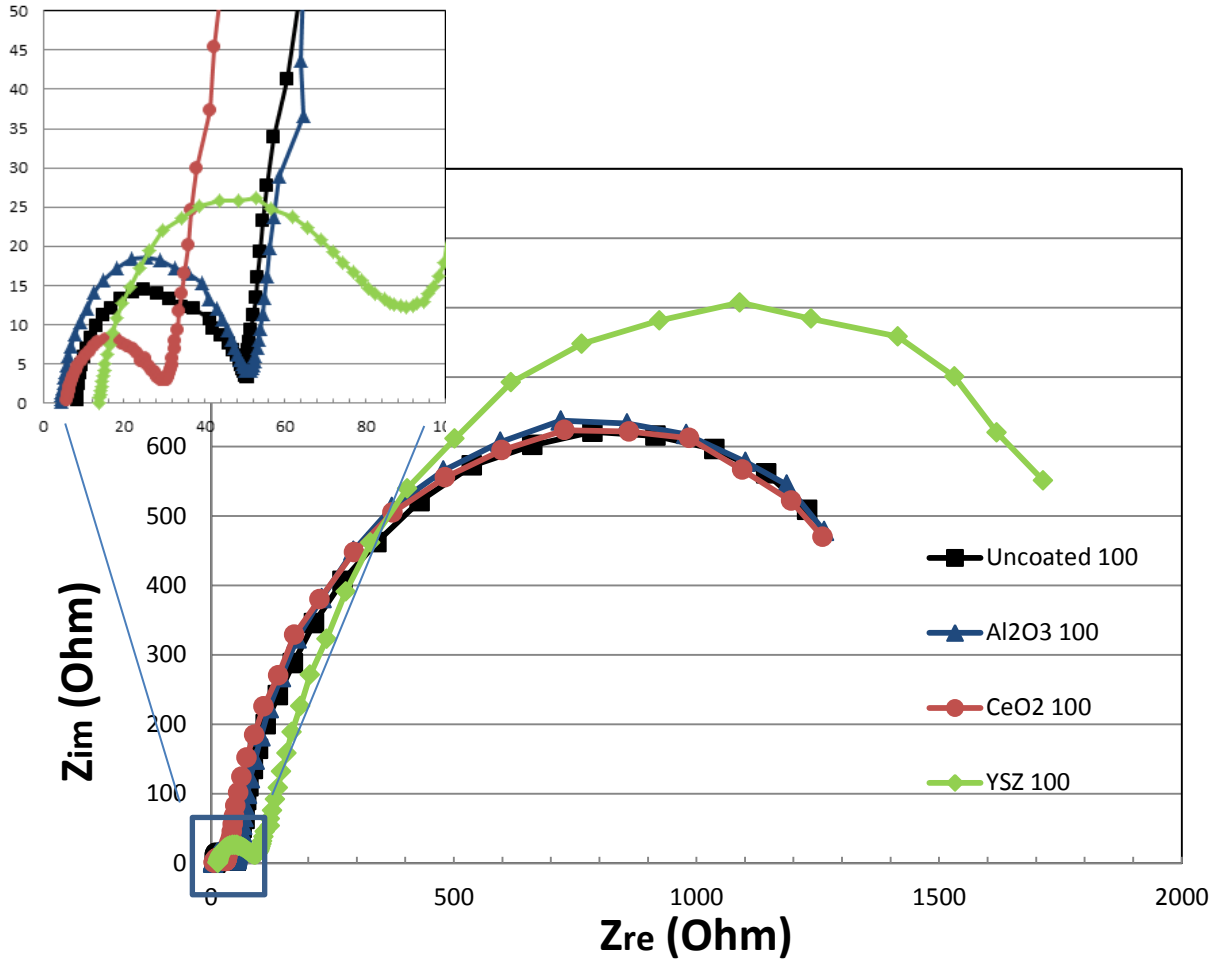

Fig. 34: EIS spectrum after repeated high voltage cycling. Charge transfer resistance is orders of magnitude larger than surface film resistance, and thus will dominate any electrical response such as capacity measurements. However, CeO_2 surface film resistance is nearly half that of the other cells.

After 100 cycles, the charge transfer resistance dominates overall resistance as seen in Fig. 34. It is still possible to view the differences between the surface film components (inset). The CeO_2 coated cell still shows the best electrochemical performance as indicated by the smallest surface film resistance after all cycling. R_{ct} for all cells has increased from electrode dissolution, HF attack, and decreased electrical contact between grains. Charge transfer resistance has also been theorized to increase

more slowly with coated materials due to the coatings' diffusion into bulk grains and stabilizing the structure, but this is not evident here [88].

Table 4: Electrochemical properties before and after high-voltage cycling.

	Uncoated	Al_2O_3	CeO_2	YSZ
R_{sf} 40 (Ohm)	31	31	27	76
R_{sf} 100 (Ohm)	43	48	26	80
R_{ct} 40 (Ohm)	102	70	66	140
R_{ct} 100 (Ohm)	~1600	~1400	~1400	~2000

Fig. 35 shows the discharge capacity retention during high voltage cycling through 40 cycles, normalized to the first cycle discharge capacity. All cells show strikingly similar performance in this regard. After 40 cycles at high voltage all cells retained about 80% of initial capacity, the commercial threshold for a dead battery. The probable reason for no visible coating effect on high voltage capacity retention is that the PLD coating of NMC grains is not conformal, nor is it of high percentage on the active material. Thus, harmful side reactions may be prevented on only small portions of active material and the grain is still corroded on other sides. Thus, in order to really show the effect of a coating, a composite cathode with more NMC by weight is suggested. The cyclical rise and fall within the overall capacity decay is mysterious, and might possibly be due to regular temperature fluctuations in the testing room.

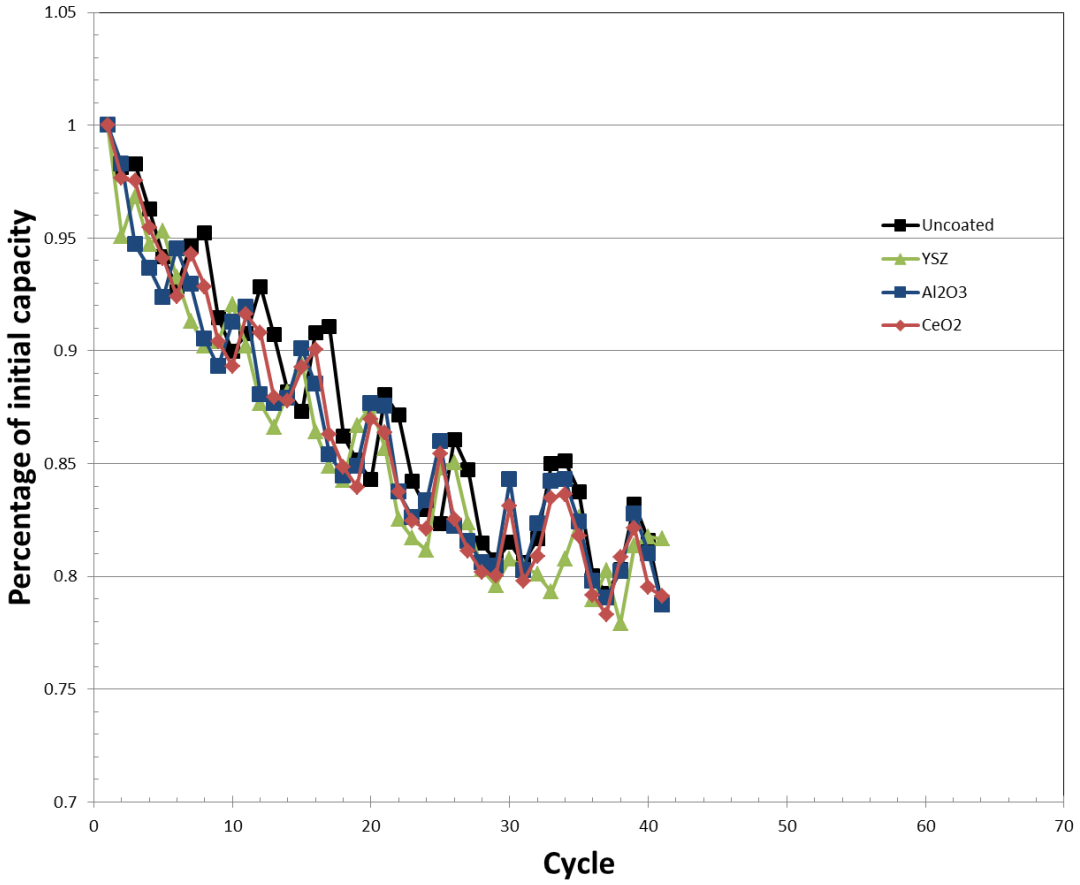

Fig. 35: Capacity retention at high rate for all cells. By percentage, the capacity loss is similar among coated and uncoated cells.

2.5.5 Cell evolution study through EIS

Using EIS results from sections 2.5.2 and 2.5.3, the electrochemical processes in the uncoated and CeO_2 coated cells were compared throughout the lifetime of each battery. Fig. 36 shows all EIS spectra for the uncoated cell superimposed on the same plot. Solution/series resistance R_e increases monotonically throughout the tests, indicating that electrolyte or contacts become more resistive upon cycling. Charge

transfer resistance also always increases but at an accelerated rate. Charge transfer resistance relies upon interfaces between grains which can be moved or dissolved by the electrolyte, and the increase becomes large after high voltage cycling where the electrolyte becomes much more reactive. Between the first and tenth cycles, the surface film resistance does not obviously increase, but only charge transfer resistance shows a change. This makes sense if after the first cycle SEI formation is complete and relatively stable throughout low voltage, low rate cycling. However, upon the 41st charge to high voltage the surface film resistance does increase noticeably as well as charge transfer resistance. Since then R_{sf} increases with cycling, indicating that at higher voltages the SEI layer is no longer static but growing in impedance.

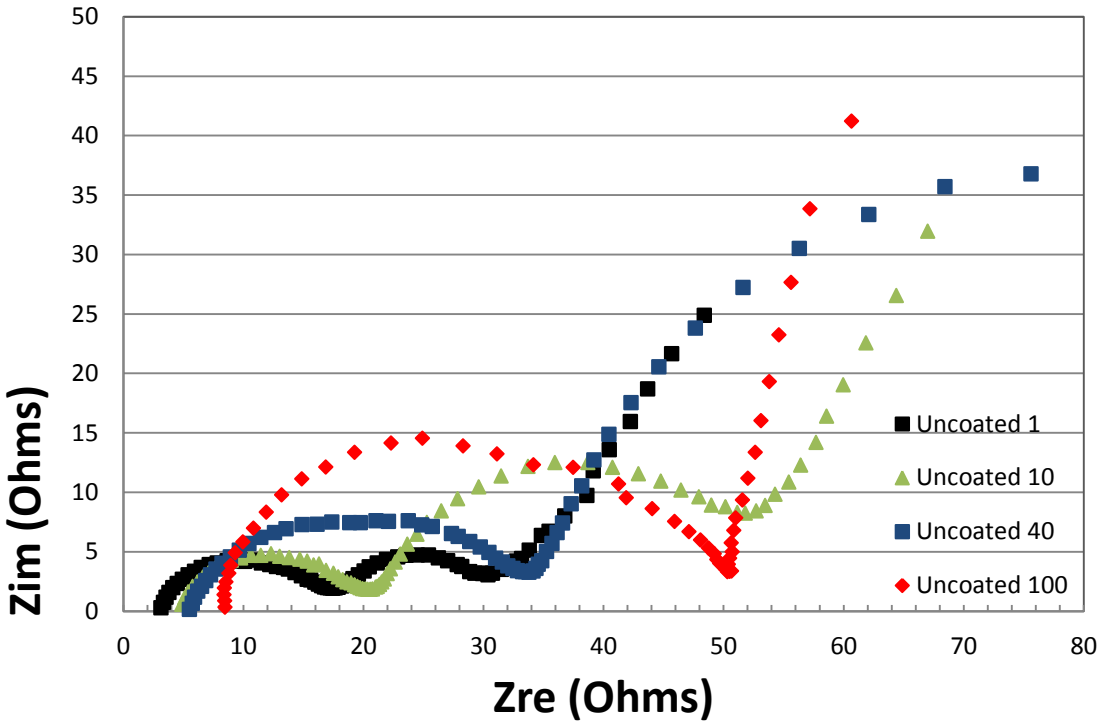

Fig. 36: EIS spectra of uncoated cell at different number of cycles displaying cell evolution.

It is more complicated for the case of the CeO_2 coated battery through EIS analysis, shown in Fig. 37. Unlike the uncoated cell, R_e does not continue to increase but fluctuates. This is not simply due to a poor connection on the first measurement, because the spectrum at 100 cycles shows the smallest contact/electrolyte resistance of all. The lack of increase could be due to the coating's effect to prevent electrolyte reactions. Again the surface film resistance increases upon high voltage cycling, but another unexplained phenomena visible in the EIS plot of the 100th cycle is the near-identical value of R_{sf} compared to 40th cycle. A further repeatability test shall be conducted for further investigation.

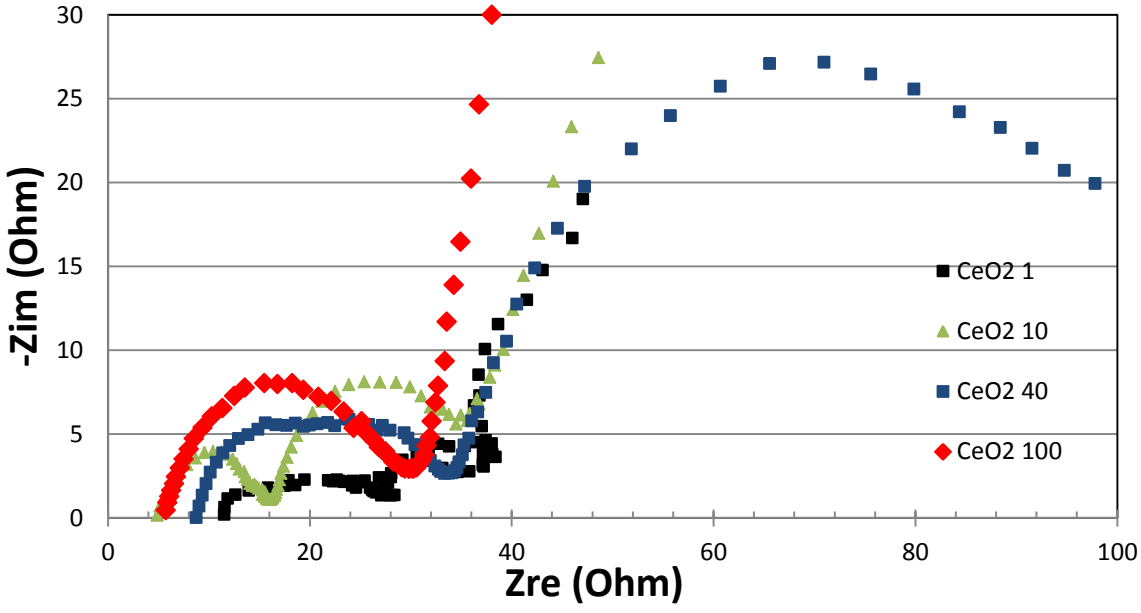

Fig. 37: EIS spectra of CeO_2 coated cell at different number of cycles displaying cell evolution.

2.6 Conclusion

Doctor blade NMC-C-PVDF cathodes were prepared and coated through PLD with Al_2O_3, CeO_2, and $Zr_{0.92}Y_{0.08}O_2$, respectively. Microstructural characterizations by TEM and SEM proved the coating and its thickness, while electrical characterization methods such as CV, GITT, and EIS compared electrochemical effects of surface coating. The CeO_2 coating enhanced overall capacity and rate performance due to its electrical conductivity and chemical inertness, while YSZ coating showed decreased performance compared to an uncoated cell. The Al_2O_3 coated cell began testing equivalent to the uncoated cell but slowly improved in performance possibly due to its chemical stability inhibiting conductive matrix dissolution. In high voltage testing, all cells increased in charge transfer resistance orders of magnitude above surface film resistance, making any improvements from coating invisible to cycling tests. Close examination of the EIS results throughout testing reveal information about the battery's electrochemical processes. Tests on optimizing the cathode composition are under way in order to maximize surface film effect visibility.

3. SUMMARY AND CONCLUSIONS

3.1 Summary

In this thesis, Lithium ion battery cathodes prepared by doctor blade method were coated with a thin layer of surface coating through pulsed laser deposition and electrically tested for rate performance and high voltage stability. The electrochemical impedance spectra of the uncoated and coated cells were measured after many different numbers of cycles to view the internal physical property variation of the cathode. Further understanding of the mechanism of rate performance enhancement and chemical protection by thin oxide coatings will continue to improve battery capability and open up new applications.

Ceria coated $LiNi_{0.5}Mn_{0.3}Co_{0.2}O_2$ showed the best capacity and rate performance in electrical testing. Through electrochemical impedance spectroscopy, the surface film resistance was found to remain after repeated cycling at high voltage. CeO_2 is proposed as an effective electrically conductive yet chemically stable coating for Lithium ion battery cathodes. Alumina coated cathode began tests with similar performance to the uncoated cell, but through the course of testing the rate capability and recoverable capacity was improved. This is possibly due to Al_2O_3's well-known abilities as HF scavenger and chemically inert nature. Yttria-stabilized Zirconia coated cathode performed worse than uncoated in terms of capacity, rate capability, and EIS-related figures of merit. The reason for such poor performance is not known, and repeatability tests are under way to verify performance. High voltage cycling revealed no difference

in irreversible loss between any coated or uncoated cells. The reason for a lack of distinction could be the relatively small percentage of surface area covered by a mostly-planar pulsed laser deposition coating.

3.2 Future Research Directions

The electrochemical effects of cathode coatings might be more effectively studied in other ways. Increasing the amount of active material coated by PLD should increase any differences to more measurable levels. One way to increase the active material coating is to create a doctor blade process with smaller amounts of Carbon and PVDF relative to NMC so that on the surface more NMC is directly coated. Also, decreasing the doctor blade film thickness would enhance the signal by allowing coated material to be a larger percentage. Tests are under way, though a large problem with changing the weight ratios is that electrical conduction between grains suffers, increasing charge transfer resistance and polarization by large amounts. As previously noted, when charge transfer resistance dwarfs surface film resistance electrical measurements are basically invariant with respect to changes in R_{sf}. Care must be taken to find a balance between Carbon percentage for electrical optimization and NMC presence for coating effect.

REFERENCES

[1] J.M. Tarascon, Philosophical Transactions of the Royal Society A: Mathematical, Physical and Engineering Sciences 368 (2010) 3227-3241.

[2] J.M. Tarascon, M. Armand, Nature 414 (2001) 359-367.

[3] M.S. Whittingham, Science 192 (1976) 1126-1127.

[4] K. Mizushima, P.C. Jones, P.J. Wiseman, J.B. Goodenough, Materials Research Bulletin 15 (1980) 783-789.

[5] M.M. Thackeray, W.I.F. David, P.G. Bruce, J.B. Goodenough, Materials Research Bulletin 18 (1983) 461-472.

[6] A.K. Padhi, K.S. Nanjundaswamy, J.B. Goodenough, Journal of the Electrochemical Society 144 (1997) 1188-1194.

[7] M. Wakihara, Materials Science and Engineering: R: Reports 33 (2001) 109-134.

[8] Y. Nishi, The Chemical Record 1 (2001) 406-413.

[9] J. Yang, M. Winter, J.O. Besenhard, Solid State Ionics 90 (1996) 281-287.

[10] X.P. Gao, J.L. Bao, G.L. Pan, H.Y. Zhu, P.X. Huang, F. Wu, D.Y. Song, The Journal of Physical Chemistry B 108 (2004) 5547-5551.

[11] P.G. Bruce, B. Scrosati, J.-M. Tarascon, Angewandte Chemie International Edition 47 (2008) 2930-2946.

[12] T. Takamura, K. Sumiya, J. Suzuki, C. Yamada, K. Sekine, Journal of Power Sources 81–82 (1999) 368-372.

[13] O. Mao, R.A. Dunlap, J.R. Dahn, Journal of the Electrochemical Society 146 (1999)

405-413.

[14] Y. Idota, T. Kubota, A. Matsufuji, Y. Maekawa, Tsutomu Miyasaka, Science 276 (1997) 1395-1397.

[15] C. Wang, Y. Zhou, M. Ge, X. Xu, Z. Zhang, J.Z. Jiang, Journal of the American Chemical Society 132 (2009) 46-47.

[16] C.K. Chan, P. Hailin, L. Gao, K. McIlwrath, Z. Xiao Feng, R.A. Huggins, C. Yi, Nature Nanotechnology 3 (2008) 31-35.

[17] M. Park, X. Zhang, M. Chung, G.B. Less, A.M. Sastry, Journal of Power Sources 195 (2010) 7904-7929.

[18] M.R. Palacin, Chemical Society Reviews 38 (2009) 2565-2575.

[19] S.S. Zhang, Journal of Power Sources 162 (2006) 1379-1394.

[20] M.S. Whittingham, Chemical Reviews 35 (2004) 4271-4301.

[21] A. Patil, V. Patil, D. Wook Shin, J.-W. Choi, D.-S. Paik, S.-J. Yoon, Materials Research Bulletin 43 1913-1942.

[22] L.J. Fu, H. Liu, C. Li, Y.P. Wu, E. Rahm, R. Holze, H.Q. Wu, Solid State Sciences 8 (2006) 113-128.

[23] C. Delmas, I. Saadoune, Solid State Ionics 53–56, Part 1 (1992) 370-375.

[24] T. Ohzuku, A. Ueda, M. Nagayama, Y. Iwakoshi, H. Komori, Electrochimica Acta 38 (1993) 1159-1167.

[25] T. Ohzuku, Y. Makimura, Chemistry Letters 30 (2001) 744-745.

[26] M. Yoshio, Y. Todorov, K. Yamato, H. Noguchi, J.-i. Itoh, M. Okada, T. Mouri, Journal of Power Sources 74 (1998) 46-53.

[27] T. Ohzuku, Y. Makimura, Chemistry Letters 30 (2001) 642-643.

[28] S.K. Martha, H. Sclar, Z. Szmuk Framowitz, D. Kovacheva, N. Saliyski, Y. Gofer, P. Sharon, E. Golik, B. Markovsky, D. Aurbach, Journal of Power Sources 189 (2009) 248-255.

[29] M. Thackeray, Nat Mater 1 (2002) 81-82.

[30] L. Dupont, M. Hervieu, G. Rousse, C. Masquelier, Palacı, M.R. Y. Chabre, J.M. Tarascon, Journal of Solid State Chemistry 155 (2000) 394-408.

[31] M.M. Thackeray, Y. Shao-Horn, A.J. Kahaian, K.D. Kepler, E. Skinner, J.T. Vaughey, S.A. Hackney, Electrochemical and Solid-State Letters 1 (1998) 7-9.

[32] T. Kakuda, K. Uematsu, K. Toda, M. Sato, Journal of Power Sources 167 (2007) 499-503.

[33] L. Xiao, Y. Zhao, Y. Yang, Y. Cao, X. Ai, H. Yang, Electrochimica Acta 54 (2008) 545-550.

[34] A. Manthiram, J.B. Goodenough, Journal of Power Sources 26 (1989) 403-408.

[35] A. Yamada, M. Hosoya, S.-C. Chung, Y. Kudo, K. Hinokuma, K.-Y. Liu, Y. Nishi, Journal of Power Sources 119–121 (2003) 232-238.

[36] S.-Y. Chung, J.T. Bloking, Y.-M. Chiang, Nat Mater 1 (2002) 123-128.

[37] W.F. Howard, R.M. Spotnitz, Journal of Power Sources 165 (2007) 887-891.

[38] F. Nobili, F. Croce, R. Tossici, I. Meschini, P. Reale, R. Marassi, Journal of Power Sources 197 (2012) 276-284.

[39] H. Sun, Y. Chen, C. Xu, D. Zhu, L. Huang, Journal of Solid State Electrochemistry 16 (2012) 1247-1254.

[40] S.-h. Wu, M.-S. Chen, C.-J. Chien, Y.-P. Fu, Journal of Power Sources 189 (2009) 440-444.

[41] G.T.-K. Fey, C.-Z. Lu, J.-D. Huang, T.P. Kumar, Y.-C. Chang, Journal of Power Sources 146 (2005) 65-70.

[42] J. Cho, Y.J. Kim, T.-J. Kim, B. Park, Angewandte Chemie 113 (2001) 3471-3473.

[43] C. Li, H.P. Zhang, L.J. Fu, H. Liu, Y.P. Wu, E. Rahm, R. Holze, H.Q. Wu, Electrochimica Acta 51 (2006) 3872-3883.

[44] Y.S. Jung, A.S. Cavanagh, A.C. Dillon, M.D. Groner, S.M. George, S.-H. Lee, Journal of the Electrochemical Society 157 (2010) A75-A81.

[45] Y. Iriyama, H. Kurita, I. Yamada, T. Abe, Z. Ogumi, Journal of Power Sources 137 (2004) 111-116.

[46] S.J. Shi, J.P. Tu, Y.J. Mai, Y.Q. Zhang, C.D. Gu, X.L. Wang, Electrochimica Acta 63 (2012) 112-117.

[47] H. Wang, Journal of the Electrochemical Society 146 (1999) 473.

[48] S.-T. Myung, N. Kumagai, S. Komaba, H.-T. Chung, Solid State Ionics 139 (2001) 47-56.

[49] C. Julien, G.A. Nazri, A. Rougier, Solid State Ionics 135 (2000) 121-130.

[50] M. Mladenov, R. Stoyanova, E. Zhecheva, S. Vassilev, Electrochemistry Communications 3 (2001) 410-416.

[51] J. Cho, Y.J. Kim, B. Park, Chemistry of Materials 12 (2000) 3788-3791.

[52] G.T.K. Fey, J.D. Huang, T.P. Kumar, Y.C. Chang, Journal of the Chinese Institute of Engineers 28 (2005) 1139-1151.

[53] Z. Wang, C. Wu, L. Liu, F. Wu, L. Chen, X. Huang, Journal of the Electrochemical Society 149 (2002) A466-A471.

[54] Y.J. Kim, T.-J. Kim, J.W. Shin, B. Park, J. Cho, Journal of the Electrochemical Society 149 (2002) A1337-A1341.

[55] J. Cho, Y.J. Kim, B. Park, Journal of the Electrochemical Society 148 (2001) A1110-A1115.

[56] Z. Chen, J.R. Dahn, Electrochemical and Solid-State Letters 5 (2002) A213-A216.

[57] Z. Wang, H. Dong, L. Chen, Y. Mo, X. Huang, Solid State Ionics 175 (2004) 239-242.

[58] S. Oh, J.K. Lee, D. Byun, W.I. Cho, B. Won Cho, Journal of Power Sources 132 (2004) 249-255.

[59] G.T.-K. Fey, C.-L. Hsiao, P. Muralidharan, Journal of Power Sources 189 (2009) 837-840.

[60] G. Ting-Kuo Fey, C.-Z. Lu, T. Prem Kumar, Y.-C. Chang, Surface and Coatings Technology 199 (2005) 22-31.

[61] X. Zhang, T.M. Devine, Journal of the Electrochemical Society 153 (2006) B375-B383.

[62] G.G. Amatucci, N. Pereira, T. Zheng, I. Plitz, J.M. Tarascon, Journal of Power Sources 81–82 (1999) 39-43.

[63] D. Arumugam, G.P. Kalaignan, Electrochimica Acta 55 (2010) 8709-8716.

[64] X. Yu, Y. Liu, G. Hu, Z. Peng, Y. Meng, Journal Wuhan University of Technology, Materials Science Edition 21 (2006) 56-59.

[65] Y.W. Tsai, R. Santhanam, B.J. Hwang, S.K. Hu, H.S. Sheu, Journal of Power Sources 119–121 (2003) 701-705.

[66] S.-W. Lee, K.-S. Kim, H.-S. Moon, H.-J. Kim, B.-W. Cho, W.-I. Cho, J.-B. Ju, J.-W. Park, Journal of Power Sources 126 (2004) 150-155.

[67] Y.-M. Lin, H.-C. Wu, Y.-C. Yen, Z.-Z. Guo, M.-H. Yang, H.-M. Chen, H.-S. Sheu, N.-L. Wu, Journal of the Electrochemical Society 152 (2005) A1526-A1532.

[68] D.W. Shin, J.-W. Choi, J.-P. Ahn, W.-K. Choi, Y.S. Cho, S.-J. Yoon, Journal of the Electrochemical Society 157 (2010) A567-A570.

[69] A.M. Kannan, A. Manthiram, Electrochemical and Solid-State Letters 5 (2002) A167-A169.

[70] Z.G. Lu, M.F. Lo, C.Y. Chung, The Journal of Physical Chemistry C 112 (2008) 7069-7078.

[71] K. Zaghib, A. Mauger, F. Gendron, C.M. Julien, Chemistry of Materials 20 (2007) 462-469.

[72] H.C. Shin, W.I. Cho, H. Jang, Electrochimica Acta 52 (2006) 1472-1476.

[73] Y.-D. Cho, G.T.-K. Fey, H.-M. Kao, Journal of Power Sources 189 (2009) 256-262.

[74] Y.-D. Li, S.-X. Zhao, C.-W. Nan, B.-H. Li, Journal of Alloys and Compounds 509 (2011) 957-960.

[75] H.H. Chang, C.C. Chang, C.Y. Su, H.C. Wu, M.H. Yang, N.L. Wu, Journal of Power Sources 185 (2008) 466-472.

[76] Y. Liu, C. Mi, C. Yuan, X. Zhang, Journal of Electroanalytical Chemistry 628 (2009) 73-80.

[77] J. Yao, F. Wu, X. Qiu, N. Li, Y. Su, Electrochimica Acta 56 (2011) 5587-5592.

[78] A.M. Hashem, A.E.A. Ghany, K. Nikolowski, H. Ehrenberg, Ionics 16 (2010) 305-310.

[79] A.M.A. Hashem, A.E. Abdel-Ghany, A.E. Eid, J. Trottier, K. Zaghib, A. Mauger, C.M. Julien, Journal of Power Sources 196 (2011) 8632-8637.

[80] H.-S. Kim, M. Kong, K. Kim, I.-J. Kim, H.-B. Gu, Journal of Power Sources 171 (2007) 917-921.

[81] S.-T. Myung, K. Izumi, S. Komaba, Y.-K. Sun, H. Yashiro, N. Kumagai, Chemistry of Materials 17 (2005) 3695-3704.

[82] D. Li, Y. Kato, K. Kobayakawa, H. Noguchi, Y. Sato, Journal of Power Sources 160 (2006) 1342-1348.

[83] Y. Kim, H.S. Kim, S.W. Martin, Electrochimica Acta 52 (2006) 1316-1322.

[84] L.A. Riley, S. Van Atta, A.S. Cavanagh, Y. Yan, S.M. George, P. Liu, A.C. Dillon, S.-H. Lee, Journal of Power Sources 196 (2011) 3317-3324.

[85] J.M. Zheng, Z.R. Zhang, X.B. Wu, Z.X. Dong, Z. Zhu, Y. Yang, Journal of the Electrochemical Society 155 (2008) A775-A782.

[86] S.B. Jang, S.H. Kang, K. Amine, Y.C. Bae, Y.K. Sun, Electrochimica Acta 50 (2005) 4168-4173.

[87] Y.J. Kang, J.H. Kim, S.W. Lee, Y.K. Sun, Electrochimica Acta 50 (2005) 4784-4791.

[88] Y. Huang, J. Chen, J. Ni, H. Zhou, X. Zhang, Journal of Power Sources 188 (2009) 538-545.

[89] S.-K. Hu, G.-H. Cheng, M.-Y. Cheng, B.-J. Hwang, R. Santhanam, Journal of Power Sources 188 (2009) 564-569.

[90] F. Wu, M. Wang, Y. Su, S. Chen, B. Xu, Journal of Power Sources 191 (2009) 628-632.

[91] J.M. Zheng, J. Li, Z.R. Zhang, X.J. Guo, Y. Yang, Solid State Ionics 179 (2008) 1794-1799.

[92] F. Wu, M. Wang, Y. Su, L. Bao, S. Chen, Electrochimica Acta 54 (2009) 6803-6807.

[93] E. Shinova, R. Stoyanova, E. Zhecheva, G.F. Ortiz, P. Lavela, J.L. Tirado, Solid State Ionics 179 (2008) 2198-2208.

[94] Z. Chen, Y. Qin, K. Amine, Y.K. Sun, Journal of Materials Chemistry 20 (2010) 7606-7612.

[95] J.W. Fergus, Journal of Power Sources 195 (2010) 939-954.

[96] Z. Chen, J.R. Dahn, Electrochemical and Solid-State Letters 6 (2003) A221-A224.

[97] H. Liu, G.X. Wang, D. Wexler, J.Z. Wang, H.K. Liu, Electrochemistry Communications 10 (2008) 165-169.

[98] O. Yamamoto, Electrochimica Acta 45 (2000) 2423-2435.

[99] L. Daza, C.M. Rangel, . Baranda, M.T. Casais, M. . Martınez, .A. Alonso, ournal of Power Sources 86 (2000) 329-333.

[100] R. Eason, Wiley Interscience, Hoboken, New Jersey, 2007, 682.

[101] T.J. Jackson, S.B. Palmer, Journal of Physics D: Applied Physics 27 (1994) 1581.

[102] S.-H. Na, H.-S. Kim, S.-I. Moon, Solid State Ionics 176 (2005) 313-317.

[103] S.H. Kang, J. Kim, M.E. Stoll, D. Abraham, Y.K. Sun, K. Amine, Journal of Power Sources 112 (2002) 41-48.

[104] T. Lynch, Research in progress.

[105] J.-M. Kim, H.-T. Chung, Electrochimica Acta 49 (2004) 937-944.